Cell

FOCAS: Transcriptome-wide screening of individual m^{6}A sites functionally dissects epitranscriptomic control of gene expression in cancer

Graphical abstract

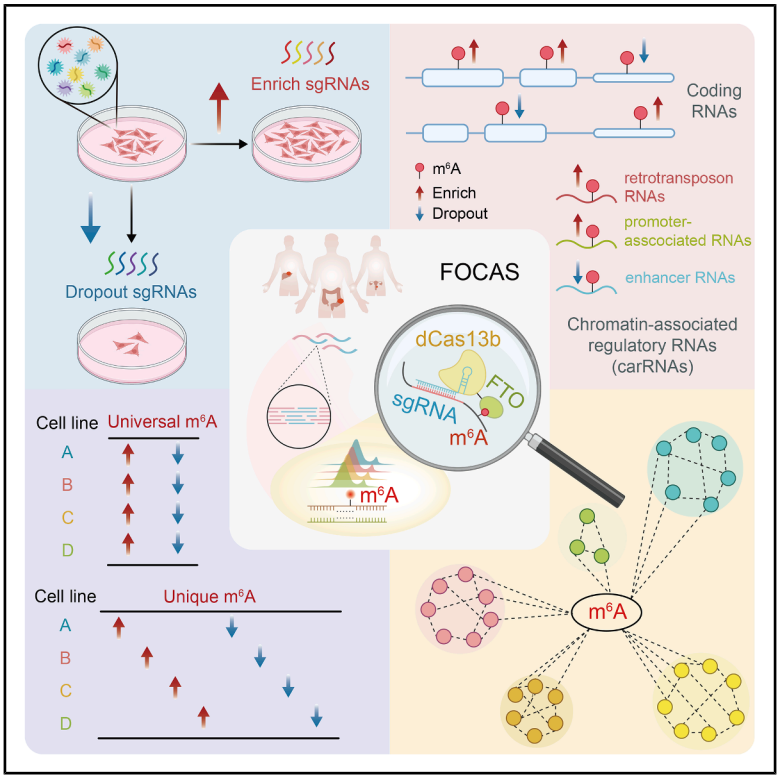

Highlights

- FOCAS reveals functional m^{6}A sites regulating cell fitness in four cancer cell lines
- Distinct m^{6}A sites within one gene exert complementary or opposing cellular functions
- Universal and cell-type-specific m^{6}A roles uncovered across diverse biological contexts
- FOCAS-validated transcription factor modules drive m^{6}A-mediated transcription control

Authors

Xinning Zhang (张薪泞), Yifan Zhang (张艺凡), Xinyu Liu (刘欣宇), ..., Yawei Gao (高亚威), Wensheng Wei (魏文胜), Jun Liu (刘君)

Correspondence

junliu1223@pku.edu.cn

In brief

We developed FOCAS as a CRISPR-based platform enabling precise, high-throughput dissection of individual m^{6}A sites across mRNA and carRNAs. It reveals RNA element-dependent m^{6}A functions within genes, illuminating the context-dependent epitranscriptomic control of gene expression in cancer.

Zhang et al., 2026, Cell *189*, 1–17
February 5, 2026
https://doi.org/10.1016/j.cell.2025.11.037

CellPress

Cell

CellPress

Resource

FOCAS: Transcriptome-wide screening of individual m^{6}A sites functionally dissects epitranscriptomic control of gene expression in cancer

Xinning Zhang (张薪泞),[1,2,9] Yifan Zhang (张艺凡),[1,2,9] Xinyu Liu (刘欣宇),[1,2,9] Chang Liu (刘畅),[3] Ying Liu (刘莹),[4] Yuan He (何苑),[5] Yuhang Qiu (邱宇航),[1] Lida Sun (孙理达),[1] Jing Hu (胡婧),[1] Yawei Gao (高亚威),[6,7,8] Wensheng Wei (魏文胜),[4,5] and Jun Liu (刘君)[1,2,8,10,*]

[1]State Key Laboratory of Gene Function and Modulation Research, School of Life Sciences, Peking-Tsinghua Center for Life Sciences, Peking University, Beijing 100871, China

[2]Beijing Advanced Center of RNA Biology (BEACON), Peking University, Beijing 100871, China

[3]Department of Genetics, Stanford University School of Medicine, Stanford, CA, USA

[4]Changping Laboratory, Beijing 102206, China

[5]Biomedical Pioneering Innovation Center, Beijing Advanced Innovation Center for Genomics, Peking-Tsinghua Center for Life Sciences, Peking University Genome Editing Research Center, State Key Laboratory of Protein and Plant Gene Research, School of Life Sciences, Peking University, Beijing 100871, China

[6]State Key Laboratory of Cardiology, Medical Innovation Center, Department of Reproductive Medicine Center, Shanghai East Hospital, Frontier Science Center for Stem Cell Research, School of Life Sciences and Technology, Tongji University, Shanghai 200092, China

[7]Frontier Science Center for Stem Cell Research, Tongji University, Shanghai 200092, China

[8]Sycamore Research Institute of Life Sciences, Shanghai 201203, China

[9]These authors contributed equally

[10]Lead contact

*Correspondence: junliu1223@pku.edu.cn

https://doi.org/10.1016/j.cell.2025.11.037

SUMMARY

Although *N*^{6}-methyladenosine (m^{6}A) is a pervasive RNA modification essential for gene regulation, dissecting the functions of individual m^{6}A sites remains technically challenging. To overcome this, we developed functional m^{6}A sites detection by CRISPR-dCas13b-FTO screening (FOCAS), a CRISPR-dCas13b-based platform enabling high-throughput, site-specific functional screening of m^{6}A. Applying FOCAS to four human cancer cell lines identified 4,475 m^{6}A-regulated genes influencing cell fitness via both mRNAs and non-coding RNAs (ncRNAs), many of which are newly linked to cancer and exhibit dynamic developmental expression. FOCAS uncovered context-dependent and reader-specific effects of m^{6}A within the same gene, revealing its intricate regulatory logic. We further uncovered universal and cell-type-specific m^{6}A patterns, with unique sites enriched in ncRNAs and universal ones in transcription-related genes. In SMMC-7721 cells, we identified m^{6}A-regulated transcriptional networks that demonstrated extensive epitranscriptome-transcriptome crosstalk. Overall, this study established a powerful, unbiased approach for the functional dissection of m^{6}A, advancing the understanding of its complexity and therapeutic relevance in cancers.

INTRODUCTION

Epitranscriptomic modifications are fundamental regulators of gene expression, essential for diverse physiological processes.[1–3] As the most prevalent internal mRNA modification, *N*^{6}-methyladenosine (m^{6}A) is installed by a multi-component methyltransferase complex and is dynamically removed by demethylases,[4] impacting nearly all aspects of mRNA processing by interacting with various reader proteins.[5–8] Beyond mRNAs, m^{6}A also occurs on specific non-coding RNAs (ncRNAs), adding another layer of transcriptional control via crosstalk with other epigenetic marks and ncRNA modulation.[9–13] Despite extensive progress, the site-specific functions of m^{6}A remain incompletely understood, orchestrated at both transcriptional and posttranscriptional levels.

Current strategies manipulating global m^{6}A levels obscure site-specific effects, limiting mechanistic and biological understanding. In cancer, core m^{6}A regulators exhibit complex and sometimes contradictory roles.[14–16] Recent studies proved that a single synonymous mutation disrupting an m^{6}A site can impact tumorigenesis,[17] highlighting the functional and therapeutic potential of site-specific regulation. Despite advances in single-base resolution m^{6}A detection,[18–20] a comprehensive functional annotation of m^{6}A sites across transcriptome remains elusive.

Please cite this article in press as: Zhang et al., FOCAS: Transcriptome-wide screening of individual m^{6}A sites functionally dissects epitranscriptomic control of gene expression in cancer, Cell (2026), https://doi.org/10.1016/j.cell.2025.11.037

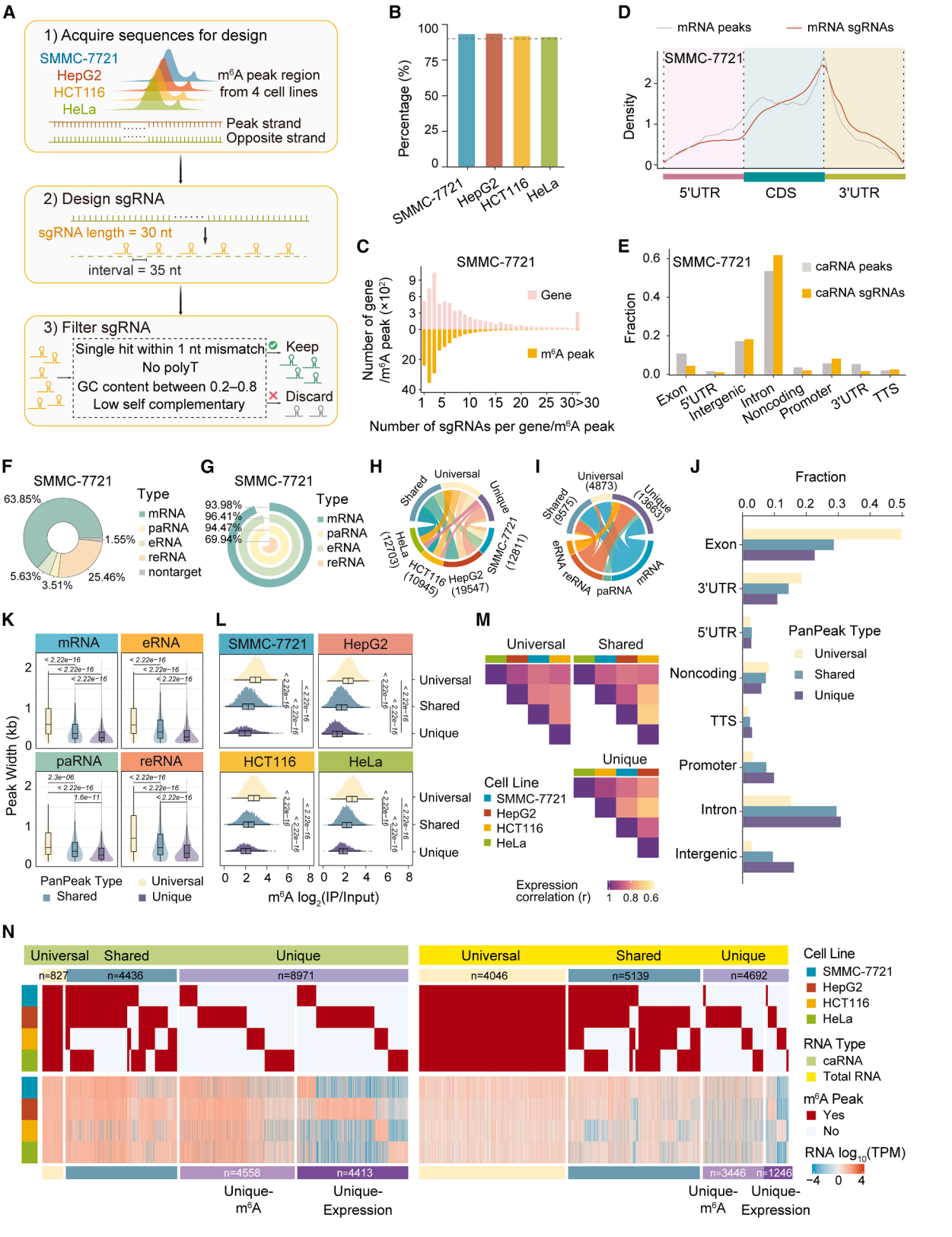

(legend on next page)

Please cite this article in press as: Zhang et al., FOCAS: Transcriptome-wide screening of individual m^{6}A sites functionally dissects epitranscriptomic control of gene expression in cancer, Cell (2026), https://doi.org/10.1016/j.cell.2025.11.037

To address this gap, we developed FOCAS (functional m^{6}A sites detection by CRISPR-dCas13b-FTO screening), a CRISPR-dCas13b system fused with fat mass and obesity-associated gene (FTO) (dCas13b-FTO)[9,21,22] that enables precise m^{6}A demethylation without genomic interference, allowing simultaneous functional analysis of m^{6}A in both mRNAs and ncRNAs. Applying FOCAS to four human cancer cell lines identified 4,475 m^{6}A-modified genes, mostly unrecognized cancer-associated genes. FOCAS demonstrated context- and reader-dependent effects of m^{6}A within individual gene, highlighting its regulatory complexity. m^{6}A regulation of cell survival exhibits both pan-cancer universality and tissue specificity. Finally, FOCAS revealed transcriptional regulatory networks modulated by m^{6}A, illuminating extensive epitranscriptome-transcriptome crosstalk. Overall, FOCAS provides a powerful and unbiased framework for functional dissection of m^{6}A, uncovering its dynamic regulatory logic and therapeutic potential.

RESULTS

Design and characterization of sgRNA libraries for FOCAS

We first evaluated the demethylation efficiency of the CRISPR-dCas13b-FTO system[9] across four cancer cell lines (SMMC-7721, HepG2, HCT116, and HeLa), using *TAF7* mRNA as a target based on its consistent methylation in m^{6}A-methylated RNA immunoprecipitation sequencing (MeRIP-seq) datasets.[23] Both real-time quantitative PCR (qPCR) following MeRIP and the single-base elongation- and ligation-based qPCR amplification (SELECT) method[24] validated the effective demethylation by sg*TAF7* targeting near the *TAF7* m^{6}A site (Figures S1A–S1E), confirming the system's reliability. Given the role of ncRNAs in chromatin organization and transcriptional regulation,[25–27] we isolated chromatin-associated RNAs (caRNAs; Figure S1F) for MeRIP-seq. m^{6}A peaks on caRNAs enriched the canonical GGACU motif, with high reproducibility between replicates (Figures S1G and S1H). Among chromatin-associated regulatory RNAs (carRNAs)—enhancer RNAs (eRNAs), promoter-associated RNAs (paRNAs), and retrotransposon RNAs (reRNAs)[9]—reRNAs exhibited the second-highest m^{6}A peak enrichment, following mRNAs (Figure S1I).

We then designed single-guide RNA (sgRNA) libraries targeting m^{6}A peaks on both mRNAs and carRNAs following rigorous quality control (Figure 1A). Qualified libraries for four cancer cell lines contained 204,832 sgRNAs targeting 12,118 genes, covering over 90% of m^{6}A-modified genes (Figure 1B; Table S2). Most genes were targeted by three sgRNAs and most m^{6}A peaks by two (Figures 1C and S1J). As expected, sgRNA distributions closely resembled those of m^{6}A peaks across both mRNAs and caRNAs (Figures 1D, 1E, S1K, and S1L). Similar to m^{6}A enrichment patterns, the libraries mostly targeted mRNAs, followed by reRNAs (Figures 1F and S1M), with high coverage across all RNA types (Figures 1G and S1N). Collectively, these sgRNA libraries enable comprehensive, unbiased targeting of m^{6}A peaks on both mRNAs and ncRNAs for subsequent functional screening.

Next, we merged m^{6}A peaks targeted by the sgRNA libraries across four cell lines into 28,111 m^{6}A PanPeaks, categorized as unique (48.6%, 13,663; one cell line), shared (34.1%, 9,575; two to three cell lines), or universal (17.3%, 4,873, all four cell lines; Figures 1H and 1I). Most shared and universal PanPeaks originated from mRNAs, while unique ones were primarily from carRNAs, especially reRNAs (Figure 1I). Correspondingly, universal PanPeaks were predominantly distributed in exons and 3′ untranslated regions (UTRs) (Figure 1J), with the largest m^{6}A peak widths and the highest m^{6}A levels (Figures 1K and 1L), a pattern consistent across all cell lines, while unique PanPeaks were more common in intronic and intergenic regions (Figure 1J).

Interestingly, RNA elements associated with universal PanPeaks showed the highest across-cell-line expression correlation, declining with decreased peak commonality (Figure 1M). mRNAs and carRNAs associated with universal PanPeaks maintained consistently high expression levels across all cell lines (Figure 1N). In contrast, unique PanPeaks were classified into two subgroups: "unique m^{6}A" (uniform expression across cell lines regardless of methylation) and "unique expression" (elevated expression in specific cell lines with methylation; Figure 1N), suggesting that unique PanPeaks are not solely dependent on RNA expression. Functional analysis of genes

Figure 1. Design and characterization of the sgRNA libraries for FOCAS

(A) Workflow for sgRNA library design.
(B) Coverage of m^{6}A-modified genes by each sgRNA library.
(C) Distribution of sgRNAs targeting each gene (top) and each m^{6}A peak (bottom) in SMMC-7721 cells.
(D) mRNA m^{6}A peaks (GEO: GSE120860) and sgRNA library distribution along transcripts in SMMC-7721 cells.
(E) Distribution fraction of caRNA m^{6}A peaks and the sgRNA library across genomic regions in SMMC-7721 cells.
(F) Proportion of sgRNAs targeting different RNA types and nontarget sgRNAs in SMMC-7721 cells.
(G) Coverage of m^{6}A peaks by the sgRNA library across different RNA types in SMMC-7721 cells.
(H) Distribution of PanPeaks across four cell lines, classified by their sharing degree: universal (all four cell lines), shared (two to three cell lines), and unique (one cell line).
(I) Distribution of PanPeaks across RNA types.
(J) Proportion of PanPeaks across distinct genomic regions.
(K) Distribution of original m^{6}A peak width across PanPeaks for each RNA type.
(L) Distribution of m^{6}A levels for original m^{6}A peaks located within PanPeak regions across four cell lines.
(M) Pearson correlation of gene element expression in PanPeaks across four cell lines.
(N) Expression level of PanPeaks from caRNA (left) and total RNA (right), grouped by PanPeak types.
Statistical significance in (K) and (L) was assessed by Wilcoxon rank-sum test.
See also Figure S1.

Please cite this article in press as: Zhang et al., FOCAS: Transcriptome-wide screening of individual m^{6}A sites functionally dissects epitranscriptomic control of gene expression in cancer, Cell (2026), https://doi.org/10.1016/j.cell.2025.11.037

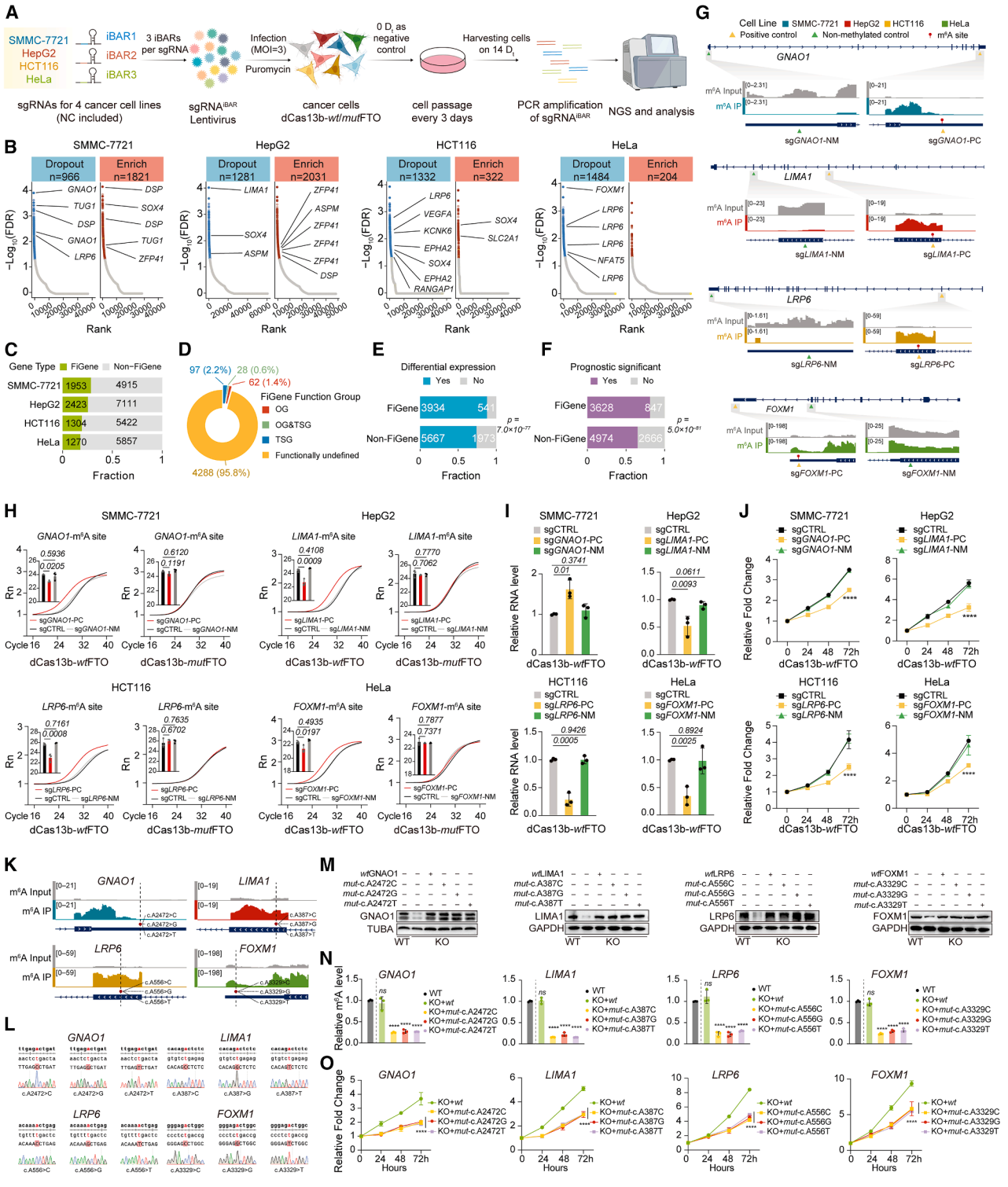

Figure 2. FOCAS workflow and characterization of effective sgRNAs

(A) Schematic of the FOCAS workflow. NC, negative control; iBAR, internal barcode; MOI, multiplicity of infection; D_t, doubling time.

(B) sgRNA ranking by robust-rank aggregation (RRA) across four cell lines expressing dCas13b-*wt*FTO. Known cancer-associated m^{6}A-modified genes are labeled.

(C) Number of FiGenes (adjusted $p < 0.05$) and non-FiGenes.

(D) Proportion of OGs or TSGs, based on Cosmic CGC,[31] among FiGenes.

(legend continued on next page)

Please cite this article in press as: Zhang et al., FOCAS: Transcriptome-wide screening of individual m^{6}A sites functionally dissects epitranscriptomic control of gene expression in cancer, Cell (2026), https://doi.org/10.1016/j.cell.2025.11.037

with unique PanPeaks revealed cell-type-specific regulatory pathways, such as phosphatidylinositol 3-kinase-protein kinase B (PI3K-Akt), c-Jun N-terminal kinase (JNK), and vascular endothelial growth factor (VEGF) signaling in SMMC-7721; metabolic pathways in HepG2; and ion channel pathways related to intestinal absorption in HCT116 (Figure S1O). Overall, our sgRNA libraries encompass both conserved and context-specific m^{6}A landscapes, with non-coding regions presenting greater cell-type specificity than coding regions.

Transcriptome-wide cell fitness screening of functional m^{6}A sites in four cancer cell lines

To enhance screening precision, we integrated sgRNA libraries with internal barcode (iBAR) adapters[28,29] and included 1,000 nontarget controls (Figures 1F and 2A). Four cell lines were engineered to stably express either CRISPR-dCas13b-*wt*FTO or its catalytically inactive counterpart (CRISPR-dCas13b-*mut*FTO) at comparable levels (Figure S2A). Cells were collected at 0 and 14 doubling times (D_t) in two biological replicates per condition for next-generation sequencing. The MAGeCK algorithm[29,30] was used to analyze sgRNA changes between 0 and 14 D_t, calculating *Z* score of $\log_2$ fold change (zLFC). Replicates in dCas13b-*wt*FTO cells showed strong consistency, while dCas13b-*mut*FTO controls displayed minimal changes and low reproducibility (Figures S2B and S2C). Overall m^{6}A levels quantified by liquid chromatography-tandem mass spectrometry (LC-MS/MS) showed no remarkable changes (Figure S2D). Targeting *TAF7* mRNA with two sgRNAs produced the most significant m^{6}A reduction at targeted sites without affecting adjacent regions (Figure S2E), confirming the specificity and reliability of dCas13b-FTO editing system with minimal off-target effects.

After removing background noise from dCas13b-*mut*FTO controls, we identified 8,926 sgRNAs (adjusted $p < 0.05$) targeting 4,475 m^{6}A-modified genes that impacted cell fitness (Figure 2B). Of these, 4,819 inhibited cell proliferation ("dropout candidates"), while 4,244 promoted cell fitness ("enrich candidates"; Figure 2B). Notably, in all cell lines, we identified that sgRNA targets included known m^{6}A-modified regulators of cell proliferation, such as *VEGFA*[35] and G protein subunit alpha O1 (*GNAO1*),[36] as well as numerous essential genes unreported to be m^{6}A-methylated (Figure 2B; Table S2). m^{6}A peaks targeted by both dropout and enrich candidates were uniformly distributed across the genome, resembling the original m^{6}A peaks, indicating minimal bias (Figures S2F and S2G). The RNA-type composition of these candidates varied across cell lines. In SMMC-7721 and HepG2, enrich candidates were less likely to target reRNAs but modestly preferred mRNAs, whereas dropout candidates reflected the library average. In contrast, HeLa and HCT116 exhibited more variations among dropout candidates (Figure S2H), indicating cancer-type-specific regulation.

The 4,475 genes targeted by effective sgRNAs, termed FOCAS-identified genes (FiGenes), represented ~20% of all targeted genes, a higher rate than Cas9 knockout screens of protein-coding genes[37] (~11%; Figure 2C), suggesting that FOCAS captures diverse m^{6}A regulatory roles across RNA species. 95.8% of FiGenes were functionally uncharacterized, with a few known oncogenes (OGs) or tumor suppressor genes (TSGs) annotated in the Cancer Gene Census (CGC) database[31] (Figure 2D). Gene Ontology (GO) analysis of FiGenes revealed enrichment of cell-cycle regulation pathways across cell lines, alongside distinct cell-type-specific processes (Figure S2I). Notably, FiGenes were more frequently differentially expressed between tumor and normal tissues, as well as more strongly associated with patient survival in The Cancer Genome Atlas (TCGA) datasets (Figures 2E and 2F). We also identified numerous m^{6}A-associated disease mutation (mDM) sites[17] within ±200 bp of effective sgRNA targets (Figure S2J). FiGenes showed a higher enrichment for cancer-associated SNPs,[38,39] compared with the overall sgRNA library (Figure S2K), emphasizing their significance in cancer.

To validate FOCAS results, we selected top-ranked dropout candidates—*GNAO1* (SMMC-7721),[36] LIM domain and actin binding 1 (*LIMA1*) (HepG2),[40] LDL receptor related protein 6 (*LRP6*) (HCT116),[41] and Forkhead box protein M1 (*FOXM1*) (HeLa)[42]—for experimental confirmation (Figure 2G). SELECT assays confirmed that dCas13b-*wt*FTO, but not dCas13b-*mut*FTO or sgRNAs targeting non-methylated regions (sg-NM), effectively reduced m^{6}A levels at targeted sites without affecting nearby non-modified sites (N sites; Figures 2H and S2L). This demethylation correlated with altered gene expression and suppressed cell proliferation (Figures 2I and 2J), consistent with reported roles of these genes.[36,40–42] No significant effects were observed with sg-NM or dCas13b-*mut*FTO (Figures 2I, 2J,

(E) Proportion of FiGenes and non-FiGenes differentially expressed in tumors versus normal tissues, based on OncoDB.[32,33]
(F) Proportion of FiGenes and non-FiGenes linked to better or worse patient survival, based on the Human Protein Atlas.[34]
(G) m^{6}A peaks on *GNAO1* (SMMC-7721), *LIMA1* (HepG2), *LRP6* (HCT116), and *FOXM1* (HeLa), with effective sgRNAs (sg*GNAO1*-PC/sg*LIMA1*-PC/sg*LRP6*-PC/sg*FOXM1*-PC, yellow) and control sg-NM regions (sg*GNAO1*-NM/sg*LIMA1*-NM/sg*LRP6*-NM/sg*FOXM1*-NM, green).
(H) SELECT-qPCR validating m^{6}A reduction at targeted sites in dCas13b-*wt*FTO or dCas13b-*mut*FTO cells with effective sgRNAs versus controls ($n = 3$).
(I and J) RT-qPCR (I) and cell counting kit-8 (CCK-8) assay (J) measuring transcript-level changes and cell proliferation in dCas13b-*wt*FTO cells with effective sgRNAs versus controls ($n = 3$, $^{****}p < 0.0001$).
(K) Integrative genomics viewer (IGV) tracks showing representative m^{6}A peaks at target sites in SMMC-7721, HepG2, HCT116, and HeLa cells.
(L) Sanger sequencing showing successful gene rescue of mutant forms of *GNAO1* (A2472C/G/T), *LIMA1* (A387C/G/T), *LRP6* (A556C/G/T), and *FOXM1* (A3329C/G/T) in corresponding knockout cells.
(M) Protein levels of GNAO1, LIMA1, LRP6, and FOXM1 in knockout cells rescued with wild type or mutant of corresponding genes.
(N) Bar plots showing m^{6}A levels at targeted sites, quantified by SELECT-qPCR, in knockout cells rescued with wild type or mutant of corresponding genes, compared with wild-type cells ($n = 3$, $^{****}p < 0.0001$).
(O) CCK-8 assay showing cell proliferation in knockout cells rescued with mutant versus wild type of corresponding genes ($n = 3$, $^{****}p < 0.0001$).
Statistical significance in (E) and (F) was determined by Fisher's exact test. Error bars indicate mean ± SD (H–J, M, and N). ns, not significant (M).
See also Figure S2.

Please cite this article in press as: Zhang et al., FOCAS: Transcriptome-wide screening of individual m^{6}A sites functionally dissects epitranscriptomic control of gene expression in cancer, Cell (2026), https://doi.org/10.1016/j.cell.2025.11.037

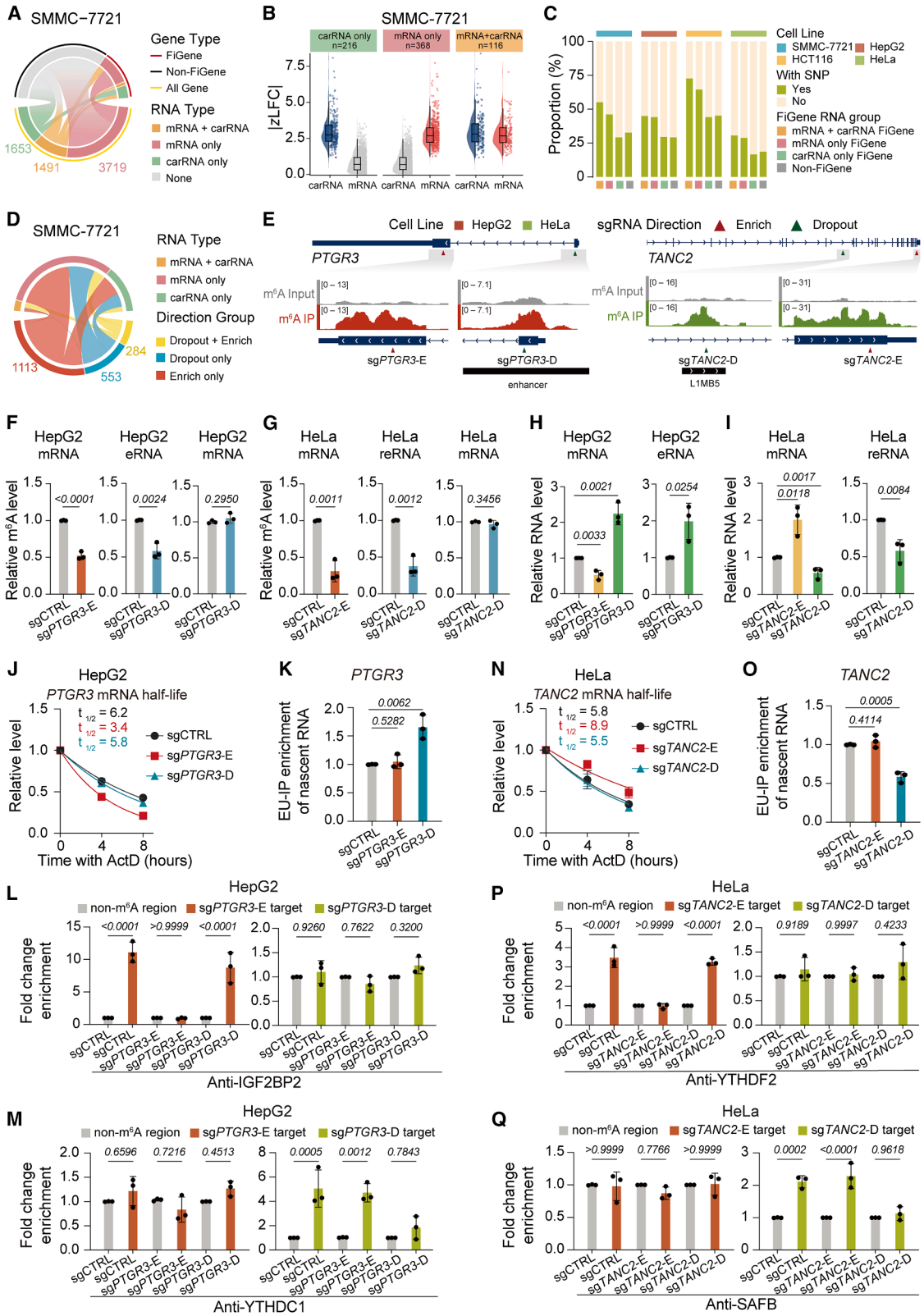

(legend on next page)

Please cite this article in press as: Zhang et al., FOCAS: Transcriptome-wide screening of individual m^{6}A sites functionally dissects epitranscriptomic control of gene expression in cancer, Cell (2026), https://doi.org/10.1016/j.cell.2025.11.037

S2M, and S2N), reinforcing the specificity of targeted demethylation.

To rigorously confirm that the phenotypes were directly attributable to m^{6}A disruption, we employed knockout-rescue experiments for these four FiGenes. Endogenous genes were knocked out and rescued with either wild-type cDNAs or point mutants that specifically disrupted original m^{6}A sites (*GNAO1*-c.A2472G/C/T, *LIMA1*-c.A387G/C/T, *LRP6*-c.A556G/C/T, *FOXM1*-c.A3329G/C/T; Figures 2K and 2L). Immunoblotting verified comparable expression between wild-type and mutant constructs, while SELECT assays confirmed that only the point mutations effectively abolished m^{6}A modification at the target sites (Figures 2M and 2N). Notably, m^{6}A-deficient mutants consistently reduced cell proliferation, mirroring the dCas13b-FTO-mediated effects (Figure 2O). Together with prior evidence that synonymous mutations at m^{6}A sites can alter biological outcomes,[17,43] our results underscore the functional significance of individual m^{6}A modifications and highlight the necessity of FOCAS for uncovering essential methylation sites.

FOCAS identifies multiplex functional m^{6}A sites and elucidates their nuanced regulatory mechanisms

mRNA m^{6}A regulates RNA processing via diverse reader proteins,[44] while carRNA m^{6}A influences chromatin accessibility and transcription.[9–13] FOCAS enables precise m^{6}A function evaluation across RNA types. Among multi-sgRNA genes, ~20%–30% were targeted by both types (Figures 3A and S3A). For FiGenes, only a small fraction was affected by both types, while others were targeted exclusively by either mRNAs or carRNAs (Figures 3A and S3A). For instance, in SMMC-7721, 700 of 1,491 dual-targeted genes were FiGenes, 116 significant for both RNA species and 584 for one (Figure 3B). This pattern, consistent across cell lines (Figure S3B), indicates that carRNA m^{6}A often acts in *trans* rather than in *cis*. Dual-species-targeted FiGenes more frequently harbored cancer-associated SNPs and included OGs or TSGs (Figures 3C and S3C). Conversely, carRNA-only FiGenes showed minimal correlation with cancer-related traits (Figures 3C and S3C), supporting a primary *trans*-regulatory role for carRNA m^{6}A. Besides, 3%–15% of FiGenes were targeted by both dropout and enrich candidates, while most were exclusively targeted by sgRNAs against mRNA alone (Figures 3D and S3D). FiGenes showing bidirectional effects were more likely to harbor cancer-associated SNPs than those with unidirectional effects (Figure S3E), indicating their functional relevance in cancer.

Pan-cell line analysis revealed that 86.9% of FiGenes were targeted by one RNA type, 11.3% by different types, and only 1.8% by both mRNAs and carRNAs (Figure S3F). Similarly, 70% of FiGenes exhibited one phenotypic direction, 25% opposite, and merely 5% both across cell lines (Figure S3G). Dually targeted FiGenes, whether by RNA type or regulatory polarity, exhibited stronger cancer relevance (Figures S3H–S3K). Collectively, these findings reveal a subset of FiGenes under multilayered and context-dependent m^{6}A regulation, reflecting an intricate regulatory architecture that appears pivotal for maintaining cellular fitness and contributing to cancer progression.

To illustrate this complexity, we examined *AMOTL1* in SMMC-7721 and *TTLL4* in HCT116 cells, each targeted by opposing mRNA sgRNAs (Figure S3L), neither previously linked to m^{6}A or cancer. All sgRNAs reduced targeted m^{6}A levels, with dropout candidates (sg*AMOTL1*-D and sg*TTLL4*-D) decreasing corresponding RNA expression and stability, while enrich candidates (sg*AMOTL1*-E) are acting oppositely (Figures S3M–S3R). These outcomes suggested involvement of distinct m^{6}A reader proteins. RNA immunoprecipitation (RIP)-qPCR confirmed that IGF2BP2 bound dropout-targeted regions (Figures S3S and S3T) to stabilize transcripts,[8] while YTHDF2 bound enrich-targeted regions (Figures S3U and S3V) to promote RNA degradation.[6] These findings validated FOCAS as a platform for dissecting site-specific, reader-dependent mRNA m^{6}A functions.

We next examined carRNA-mediated regulation in HepG2 (*PTGR3*) and HeLa (*TANC2*), where two sgRNAs elicited opposite effects per gene. *PTGR3* targeting involved mRNA (sg*PTGR3*-E) and adjacent eRNA (sg*PTGR3*-D); *TANC2* involved mRNA (sg*TANC2*-E) and proximal L1 (sg*TANC2*-D; Figure 3E). All sgRNAs efficiently reduced m^{6}A levels at targeted regions (Figures 3F and 3G). sg*PTGR3*-E decreased *PTGR3* expression, while sg*PTGR3*-D increased both eRNA and *PTGR3* expression (Figure 3H), suggesting tumor-suppressive activity. Similarly, sg*TANC2*-E elevated *TANC2* mRNA, whereas sg*TANC2*-D

Figure 3. FOCAS identifies novel functional m^{6}A sites and reveals subtle regulatory mechanisms

(A) Distribution of RNA types targeted by multiple sgRNAs within the same gene across FiGenes and non-FiGenes in SMMC-7721 cells.

(B) Absolute value of *Z* scores of |zLFC| for sgRNAs targeting carRNAs or mRNAs within FiGenes in SMMC-7721 cells. FiGenes are grouped by effective sgRNA RNA type.

(C) Proportion of FiGenes containing cancer-related SNPs grouped by effective sgRNA RNA types across four cell lines.

(D) Distribution of sgRNA RNA types and direction types for FiGenes in SMMC-7721 cells.

(E) m^{6}A peaks on *PTGR3* (HepG2) and *TANC2* (HeLa), with effective sgRNAs (enrich: sg*PTGR3*-E/sg*TANC2*-E, red; dropout: sg*PTGR3*-D/sg*TANC2*-D, green).

(F–I) Methylation (F and G) and transcript (H and I) levels of *PTGR3* (F and H) and *TANC2* (G and I) were measured by MeRIP-qPCR and RT-qPCR in dCas13b-*wt*FTO cells transfected with corresponding sgRNAs versus nontarget sgRNA ($n = 3$).

(J and K) *PTGR3* mRNA's half-life (J) and nascent RNA synthesis (K) were measured by RT-qPCR after actinomycin D treatment and 5-ethynyl uridine (EU) labeling in HepG2-dCas13b-*wt*FTO cells with sgRNAs targeting *PTGR3* versus nontarget sgRNA ($n = 3$).

(L and M) The binding of IGF2BP2 (L) and YTHDC1 (M) to specific *PTGR3* regions was measured by fragmented RIP-qPCR in HepG2-dCas13b-*wt*FTO cells with sgRNAs targeting *PTGR3* versus nontarget sgRNA, comparing the enrichment at the targeted m^{6}A regions versus non-methylated regions ($n = 3$).

(N and O) *TANC2* mRNA's half-life (N) and nascent RNA synthesis (O) were assessed by RT-qPCR after actinomycin D treatment and EU labeling in HeLa-dCas13b-*wt*FTO cells with sgRNA targeting *TANC2* versus nontarget sgRNA ($n = 3$).

(P and Q) The binding of YTHDF2 (P) and SAFB (Q) to specific *TANC2* regions was assessed by fragmented RIP-qPCR in HeLa-dCas13b-*wt*FTO cells with sgRNAs targeting *TANC2* versus nontarget sgRNA, comparing the enrichment at the targeted m^{6}A regions versus non-methylated regions ($n = 3$).

Error bars indicate mean ± SD (F–Q).

See also Figure S3.

Please cite this article in press as: Zhang et al., FOCAS: Transcriptome-wide screening of individual m^{6}A sites functionally dissects epitranscriptomic control of gene expression in cancer, Cell (2026), https://doi.org/10.1016/j.cell.2025.11.037

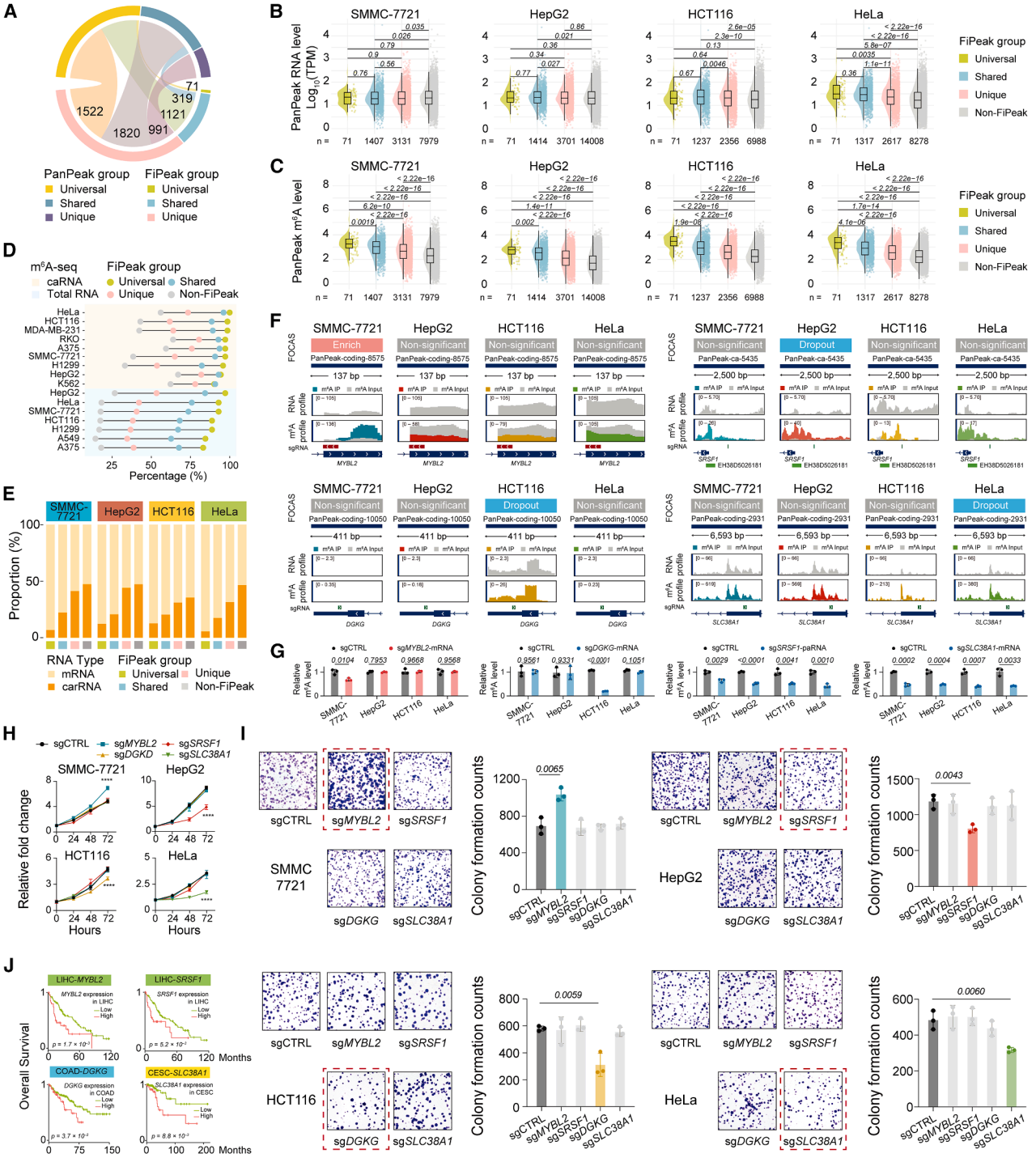

Figure 4. Universal and unique PanPeaks across four cell lines

(A) Distribution of FiPeak types across PanPeaks types.

(B and C) RNA expression (B) and m^{6}A levels (C) of FiPeaks across the four cell lines. Statistical significance was assessed using the Wilcoxon rank-sum test.

(D) Percentage of m^{6}A peaks occurrences in PanPeak regions, grouped by FiPeak types, across various cancer cell lines.

(E) Proportion of PanPeak RNA types, grouped by FiPeak types, across the four cell lines.

(F) RNA levels and m^{6}A profiles within unique PanPeaks: PanPeak-coding-8575 associated with *MYBL2* mRNA, PanPeak-ca-5435 in the *SRSF1* promoter region, and PanPeak-coding-10050 associated with the *DGKG* 3′ UTR region, PanPeak-coding-2931 in the *SLC38A1* 3′ UTR region, across four cell lines.

(legend continued on next page)

Please cite this article in press as: Zhang et al., FOCAS: Transcriptome-wide screening of individual m^{6}A sites functionally dissects epitranscriptomic control of gene expression in cancer, Cell (2026), https://doi.org/10.1016/j.cell.2025.11.037

reduced both L1 and *TANC2* transcripts (Figure 3I), indicating oncogenic potential.

Further investigation revealed that sg*PTGR3*-E shortened *PTGR3* mRNA half-life, while sg*PTGR3*-D increased its transcription and eRNA abundance (Figures 3J, 3K, and 3H). RIP-qPCR confirmed IGF2BP2 bound at sg*PTGR3*-E site, while YTHDC1 bound at sg*PTGR3*-D eRNA site (Figures 3L and 3M), which destabilizes m^{6}A-modified eRNA and suppresses nearby gene transcription.[45–47] Both interactions weakened after sgRNA treatment, matching the reduced mRNA stability and enhanced transcription (Figures 3L and 3M). Similarly, sg*TANC2*-E increased mRNA half-life, while sg*TANC2*-D suppressed its transcription and L1 expression (Figures 3I, 3N, and 3O). RIP-qPCR revealed that YTHDF2 bound the sg*TANC2*-E mRNA region (Figure 3P), while SAFB bound the L1 region targeted by sg*TANC2*-D (Figure 3Q), stabilizing the L1 and facilitating nearby gene transcription.[48] The discovery of diverse individual-m^{6}A regulatory modes within the same gene confirmed roles of distinct m^{6}A reader proteins, establishing FOCAS as a reliable approach for pinpointing functional m^{6}A sites and elucidating the m^{6}A multiplex regulatory mechanisms.

FOCAS identified unique and universal m^{6}A peaks that influence cancer cell growth

Beyond gene-level analyses, we examined the overlap and specificity of m^{6}A peaks across cell lines. Of the 28,111 m^{6}A PanPeaks designed (Figure 1H), 5,844 contained effective sgRNAs in at least 1 cell line and were termed FOCAS-identified PanPeaks (FiPeaks). Among these, 74% (4,333) was unique to a single cell line (unique FiPeaks), 25% (1,440) was shared across two to three cell lines (shared FiPeaks), and only ~1% (71) was targeted in all four (universal FiPeaks; Figure 4A). Unique FiPeaks exhibited stronger effects on cell fitness (higher |zLFC|) in all cells except HCT116 (Figure S4A). Despite comparable RNA expression, unique FiPeaks displayed lower m^{6}A levels than shared or universal FiPeaks (Figures 4B and 4C). Conversely, universal FiPeaks showed higher modification levels and frequency across tumors (Figure 4D), suggesting conserved cancer regulatory roles. We further classified FiGenes by cross-cell screening results. Universal FiGenes, shared by all cell lines, were more enriched for OGs and TSGs and strongly associated with cancer-related SNPs, differential expression, and patient prognosis (Figures S4B–S4E). They were often regulated by multi-type sgRNAs with bidirectional impacts (Figures S4F and S4G), highlighting complex m^{6}A-mediated cancer regulation.

Unique FiPeaks were enriched for carRNAs (~50%), emphasizing the distinct role of m^{6}A in ncRNA-mediated, cell-type-specific regulation (Figure 4E). Interestingly, most unique FiPeaks originated from shared or universal PanPeaks, suggesting that conserved m^{6}A patterns can exert cell-type-specific functions (Figure 4A). Further analysis revealed that unique FiPeaks derived from conserved PanPeaks showed minimal variations in m^{6}A or RNA abundance between effective and non-effective cell lines (Figures S4H–S4J), indicating that functional specificity arises from cellular context rather than differences in methylation or RNA expression levels. Across human tissues,[49] the m^{6}A frequency of FiPeaks ranked highest for universal FiPeaks and lowest for unique FiPeaks (Figure S4K). Expression dynamics during development showed that universal and shared FiGenes were highly expressed in early development but declined afterward, whereas unique FiGenes increased in later stages (Figure S4L), suggesting early proliferative roles for universal FiGenes and organ-specific functions for unique FiGenes.

We validated FiPeak cell-type specificity using PanPeak-coding-8575 (*MYBL2*, SMMC-7721) and PanPeak-coding-10050 (*DGKG*, HCT116; Figure 4F), which displayed specific methylation in corresponding cell lines. Targeting PanPeak-coding-8575 promoted cancer phenotypes exclusively in SMMC-7721 cells, while targeting PanPeak-coding-10050 specifically suppressed growth in HCT116 cells (Figures 4G–4I). Testing two additional unique FiPeaks with comparable m^{6}A levels (PanPeak-ca-5435 on a paRNA upstream of *SRSF1* and PanPeak-coding-2931 on *SLC38A1*) also yielded cell-type-specific growth effects (Figures 4F–4I), confirming that unique FiPeak identification reflects functional specificity rather than methylation abundance. All four FiGenes corresponding to these unique FiPeaks were significantly associated with patient survival (Figure 4J), underscoring their tumor-specific relevance.

Comparative analysis showed that the two liver cancer cell lines exhibited the highest FiGenes similarity (Figure S4M). Among their FiPeak-shared FiGenes, 74% displayed either opposing or minimal fitness effects in non-liver cell lines (Figure S4N), suggesting liver-specific regulation. The concordance ranking of liver cancer-shared FiGenes (see STAR Methods for details) revealed that most top-ranked genes exhibit significant liver cancer-normal differential expression and strong survival association (Figure S4O), including known regulators such as *JPT2*,[50] *GPATCH4*,[51] and *GAB2*.[52] To validate liver-specific m^{6}A regulation, we selected three high-concordance FiPeaks (Panpeak-coding-13061, *ANKRD18A*; Panpeak-coding-4726, *JPT2*; Panpeak-ca-12172, reRNA near *CDK14*), with all FiGenes associated with survival in liver cancer (Figures S4P–S4S). sgRNA treatment affected liver cancer cell lines only (Figures S4T–S4V). Specifically, PanPeak-coding-13061, classified as a universal PanPeak (Figure S4Q), further supported that FOCAS-identified liver-specific regulation arises from functional context rather than solely m^{6}A-level differences.

Universal FiGenes exert consistent effects on cell fitness through m^{6}A regulation

We next focused on the 141 universal FiGenes whose sgRNA targeting impacted cell fitness across four cancer cell lines.

(G–I) MeRIP-qPCR (G), CCK-8 (H), and colony formation (I) assays measuring m^{6}A levels and cell proliferation in cells transfected with sg*MYBL2*-mRNA, sg*DGKG*-mRNA, sg*SRSF1*-paRNA, or sg*SLC38A1*-mRNA versus nontarget sgRNA across four cell lines (n = 3, ****p < 0.0001, error bars indicate mean ± SD).
(J) Kaplan-Meier disease-free survival for patients with liver hepatocellular carcinoma (LIHC), colon adenocarcinoma (COAD), and cervical squamous cell carcinoma and endocervical adenocarcinoma (CESC), stratified by *MYBL2*, *SRSF1*, *DGKG*, and *SLC38A1* expression, respectively (Benjamini-Hochberg-adjusted log-rank test). Sample sizes (high-low expression): LIHC, n = 142–142; COAD, n = 213–213; CESC: n = 71–71.
See also Figure S4.

Please cite this article in press as: Zhang et al., FOCAS: Transcriptome-wide screening of individual m^{6}A sites functionally dissects epitranscriptomic control of gene expression in cancer, Cell (2026), https://doi.org/10.1016/j.cell.2025.11.037

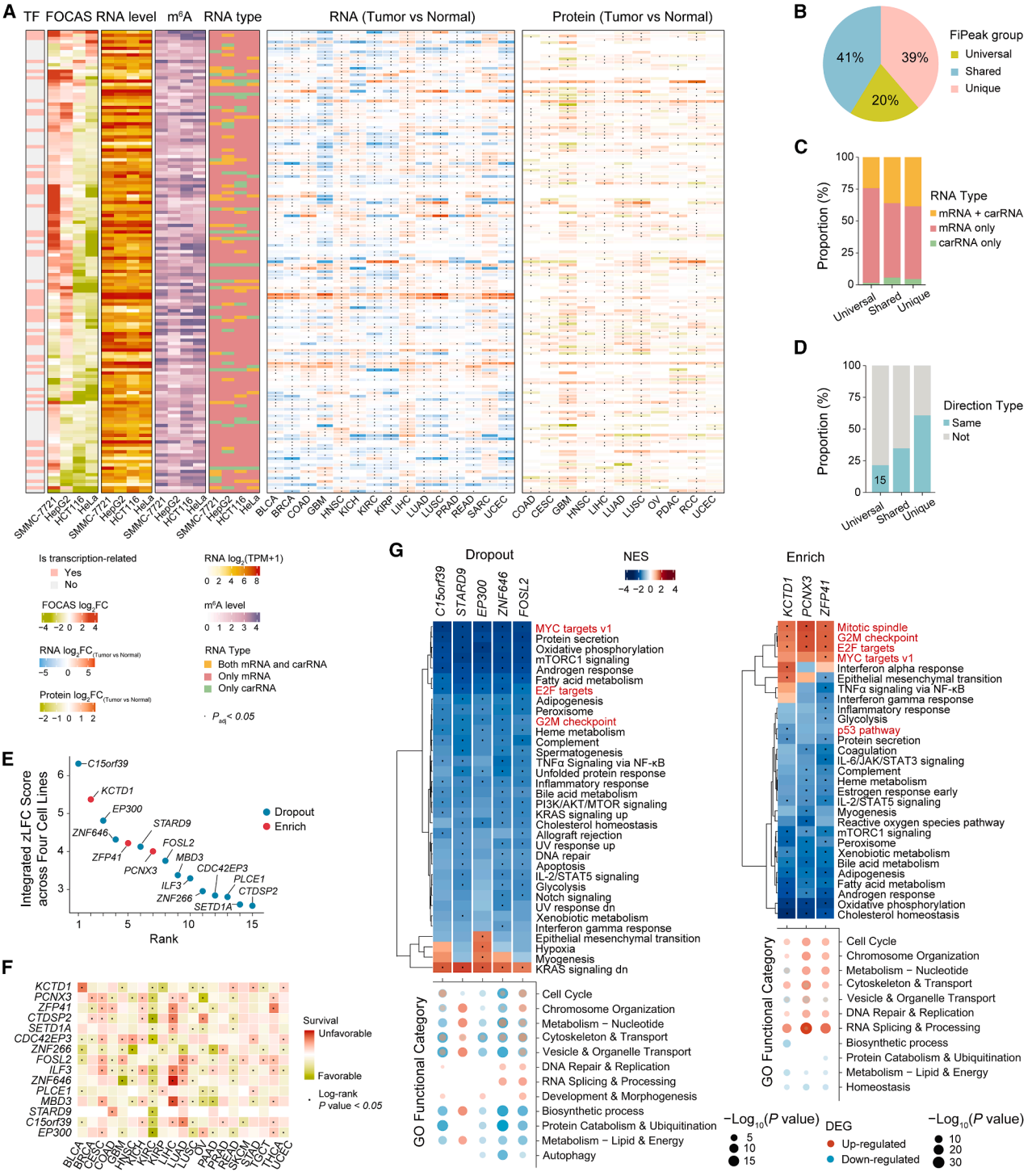

Figure 5. Universal FiGenes exert consistent effects on cell fitness through m^{6}A regulation

(A) Heatmap showing transcriptional relationships, FOCAS zLFC, RNA expression, m^{6}A levels, sgRNA RNA types, and fold changes of RNA expression and protein expression between tumor and normal tissues for universal FiGenes, based on OncoDB and CPTAC data. Statistical significance was determined by *t* test (OncoDB) or Wilcoxon rank-sum test (CPTAC) with Bonferroni correction.

(B) Pie chart showing the proportion of FiPeak types on universal FiGenes.

(C) Proportion of RNA types for universal FiGenes, grouped by FiPeak types.

(D) Proportion of FiGenes with consistent versus inconsistent screening directionality across four cell lines, grouped by FiPeak types.

(E) Integrated zLFC score for universal FiPeaks with consistent directionality across four cell lines.

(legend continued on next page)

Please cite this article in press as: Zhang et al., FOCAS: Transcriptome-wide screening of individual m^{6}A sites functionally dissects epitranscriptomic control of gene expression in cancer, Cell (2026), https://doi.org/10.1016/j.cell.2025.11.037

The two liver cancer cell lines exhibited greater regulatory concordance than HCT116 and HeLa, reflecting variable screening outcomes (Figure 5A, group "FOCAS"). These FiGenes, predominantly targeted on mRNAs, exhibited variation in RNA and m^{6}A levels across cell lines, suggesting context-dependent m^{6}A regulation (Figure 5A, groups "RNA type," "RNA level," and "m^{6}A"). Public datasets from OncoDB[32,33] and Clinical Proteomic Tumor Analysis Consortium (CPTAC)[53] revealed significant RNA and protein expression differences between tumor and normal tissues, underscoring their pan-cancer relevance (Figure 5A, right two).

FiPeaks associated with these universal FiGenes were mostly unique or shared FiPeaks, indicating that most universal FiGenes were not regulated through the same peak (Figure 5B). The unique FiPeaks showed higher representation of sgRNAs targeting carRNAs and displayed more uniform screening directions across cell lines (Figures 5C and 5D), suggesting context-specific yet functionally coherent regulation. In contrast, only around 20% of FiPeaks on universal FiGenes were classified as universal, predominantly associated with sgRNAs targeting mRNAs (Figures 5B and 5C). Fifteen universal FiPeaks exerted consistent effects across all four cell lines, highlighting their core regulatory roles in m^{6}A-mediated gene control. We derived an integrated *z*LFC score to rank their functional impact (see STAR Methods for details), with *C15orf39*- and *KCTD1*-associated FiPeaks ranking highest in the dropout and enrich direction, respectively (Figure 5E). These FiGenes were significantly correlated with patient prognosis in up to 21 cancer types, emphasizing their conserved and clinically relevant functions (Figure 5F).

To explore how these FiPeaks influence cell fitness, we selected eight top candidates for RNA sequencing (RNA-seq) following sgRNA treatment. Gene set enrichment analysis (GSEA) using MsigDB Hallmark gene sets[54] revealed that dropout sgRNAs downregulated cell cycle and proliferation pathways, while enrich sgRNAs upregulated them (Figure 5G, top). GO analysis of shared differentially expressed genes (DEGs) also confirmed that genes downregulated in the dropout group and upregulated in the enrich group were consistently enriched for cell-cycle-related functions (Figure 5G, bottom). This regulatory pattern aligns with our screening data, reinforcing the role of m^{6}A-mediated FiGene regulation in cancer cell proliferation. Functional validation of four top FiPeaks (*C15orf39*, *EP300*, *KCTD1*, and *ZFP41*) demonstrated that targeted demethylation reduced m^{6}A levels and modulated cancer phenotypes across cell lines (Figures S5A–S5G). Altogether, FOCAS identified conserved and functionally validated m^{6}A sites, with potential as universal therapeutic targets.

The m^{6}A-dependent transcription regulatory networks involved in cancer cell fitness

GO analysis showed that universal FiGenes were highly enriched in chromatin organization and transcription regulation pathways (Figure 6A). Given the critical role of aberrant transcription in tumorigenesis[55] and its potential interplay with m^{6}A,[56,57] we investigated their crosstalk using FOCAS. Approximately 40% of universal FiGenes were directly involved in transcription regulation (Figure S6A), with 25% in each cell line contributing to transcription-related processes (Figure 6B). Notably, 55%–85% had not been previously linked to the corresponding cancer, and roughly 80% lacked prior association with m^{6}A regulation (Figure S6B).

Next, we performed protein-protein interaction (PPI) analysis of transcription-related FiGenes in SMMC-7721 as a representative cell line for in-depth study (Figure S6C). Thirteen representatives were selected, most of which regulate histone modifications and transcription processes (Figure 6C). RNA-seq analysis of sgRNA-treated cells clustered them into four distinct modules: two targeted by enrich candidates (E1 and E2) and two by dropout candidates (D1 and D2; Figures 6D and S6D). D1 module exclusively comprised the histone acetyltransferase binding to ORC1 (HBO1) complex members,[58] while the others contained previously unlinked transcription regulators. Clustering of DEGs revealed five expression trends, with E2 and D2 showing contrasting transcriptional profiles, particularly in DEG clusters 1, 4, and 5 (Figure 6E). These results indicate that coordinated m^{6}A-dependent regulation of multiple transcription-related FiGenes drives distinct expression patterns, providing a compelling framework to study how m^{6}A shapes transcriptional networks.

We then investigated the m^{6}A-mediated transcription regulation using the E1 module, comprising three genes (*SETD1B*, *INTS11*, and *KCTD1*) not previously associated with liver cancer or m^{6}A modification (Figure 6E). E1-sgRNA treatment in SMMC-7721 cells significantly reduced m^{6}A levels and enhanced cancer phenotypes (Figures S5B, S5E–S5G, and S6E–S6M). *SETD1B*[59] and *INTS11*,[60] both of which are associated with H3K4me3 and transcription regulation, showed increased H3K4me3 level following sgRNA treatment (Figures 6F–6I). Interestingly, *KCTD1*, a transcription suppressor,[61,62] not previously connected to these complexes or H3K4me3 dynamics, also modulated H3K4me3 levels (Figures 6F–6I, S6N, and S6O), indicating a coordinated regulatory mechanism among E1 FiGenes through H3K4me3 modulation.

Although *KCTD1* remains poorly characterized in cancer, it emerged as the top-ranked enrich gene targeted by universal FiPeaks across four cell lines. *KCTD1* knockdown elevated H3K4me3 levels and enhanced cancer phenotype, while reintroducing KCTD1 reversed these effects (Figures S6P–S6W).

(F) Prognostic significance for FiGenes harboring universal FiPeaks with consistent directionality across 21 tumor types, based on the Human Protein Atlas.[34] *p* values were determined by the log-rank test; $p < 0.05$ was considered significant.

(G) Top: heatmaps displaying normalized enrichment scores (NESs) from GSEA based on average *z*LFCs in cells treated with dropout (left) or enrich (right) candidates versus nontarget sgRNA. Proliferation-associated MsigDB Hallmark pathways[54] are labeled in red. Bottom: dot plots showing grouped GO terms enriched among common DEGs (Benjamini-Hochberg adjusted $p < 0.05$, $|\log_2 FC| > 1$) in cells treated with dropout (left) and enrich (right) candidates. Functional categories were manually curated by clustering GO term keywords. Color denotes DEG direction: red for upregulated, blue for downregulated.

See also Figure S5.

Please cite this article in press as: Zhang et al., FOCAS: Transcriptome-wide screening of individual m^{6}A sites functionally dissects epitranscriptomic control of gene expression in cancer, Cell (2026), https://doi.org/10.1016/j.cell.2025.11.037

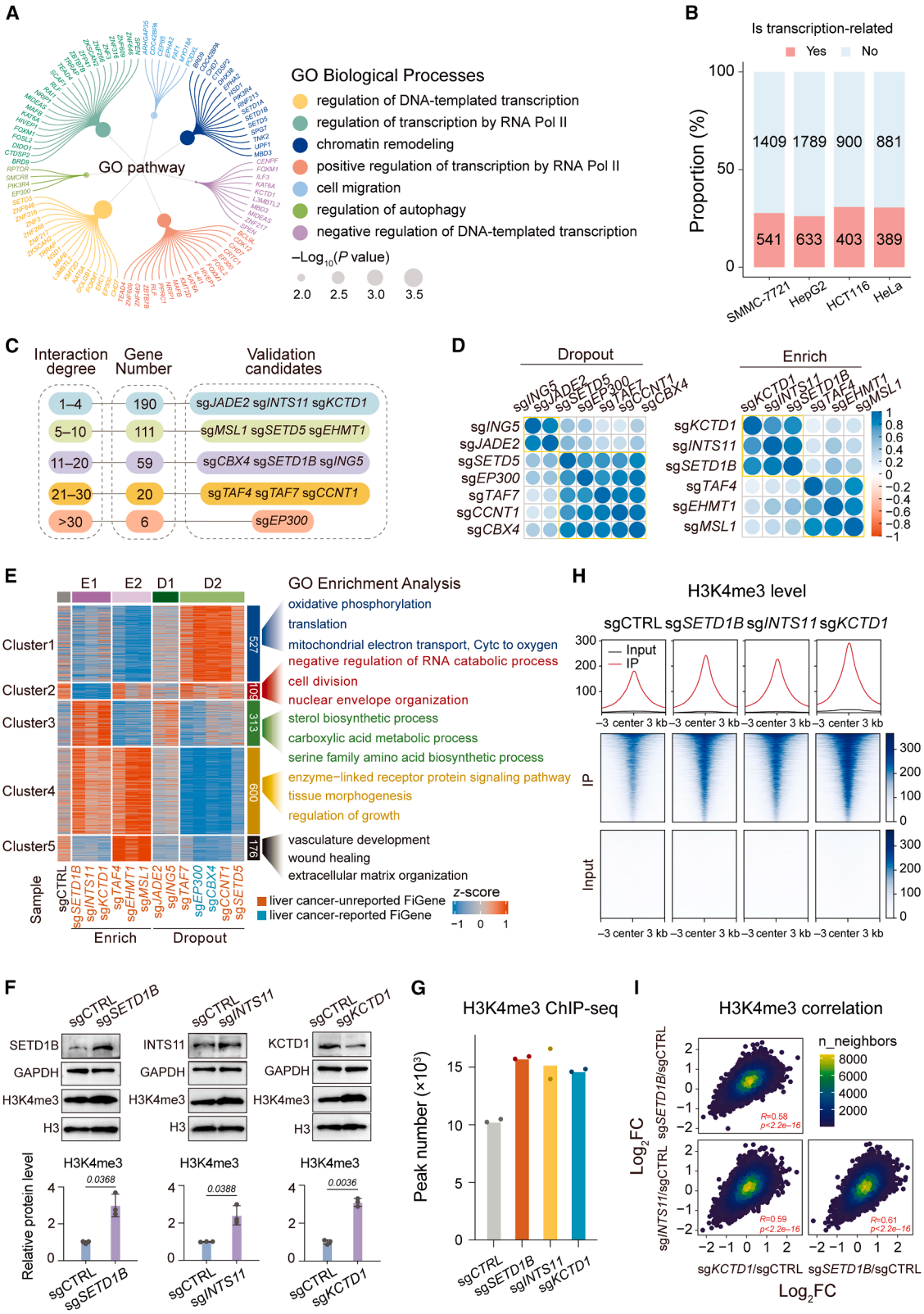

(legend on next page)

Please cite this article in press as: Zhang et al., FOCAS: Transcriptome-wide screening of individual m^{6}A sites functionally dissects epitranscriptomic control of gene expression in cancer, Cell (2026), https://doi.org/10.1016/j.cell.2025.11.037

Together, our data establish *KCTD1* as an m^{6}A-unreported FiGene with pan-cancer tumor suppressor potential, showcasing the power of FOCAS to uncover functionally relevant, uncharacterized targets and highlighting the intricate crosstalk between m^{6}A and epigenetic regulation in cancer.

DISCUSSION

The diverse functions of m^{6}A modifications demand a precise understanding of individual m^{6}A sites.[1–3] Here, we developed FOCAS, a high-throughput platform identifying 4,475 fitness-associated FiGenes across four cancer cell lines. By targeting m^{6}A on both mRNAs and ncRNAs, FOCAS uncovered how different m^{6}A sites within the same gene exert distinct effects through specific reader proteins. Notably, cell-line-specific m^{6}A peaks and FiPeaks were preferentially enriched on carRNAs over mRNAs. Moreover, we uncovered m^{6}A-transcriptional regulator networks, including *KCTD1* as an unreported, m^{6}A-regulated tumor suppressor associated with H3K4me3. Altogether, FOCAS enables functional m^{6}A site annotation, revealing fine-tuned regulatory functions and mechanisms of m^{6}A in cancer and beyond.

The power of FOCAS lies in its ability to precisely manipulate m^{6}A sites without perturbing global methylation, offering advantages over conventional approaches. FOCAS simultaneously targets >90% of m^{6}A-modified genes and most carRNAs, supporting comprehensive analysis of m^{6}A regulation in complex systems. Recent studies show that single m^{6}A-site synonymous mutations disrupt RNA structures or functions, driving tumorigenesis[17] or altering crop traits,[43] highlighting the urgent need for systematic functional dissection. With FOCAS, we identified numerous m^{6}A-modified sites whose removal affected cancer cell fitness, providing robust and large-scale evidence that discrete m^{6}A marks function as precise regulatory elements. FOCAS further uncovered m^{6}A's versatility; even within the same gene, m^{6}A on different RNA elements can exert opposing impacts via distinct readers. Systematic analysis demonstrated functional equivalence between m^{6}A on carRNAs and mRNAs, with most effects occurring in *trans*, consistent with recent studies.[63] This layered, context-dependent regulatory complexity redefines our understanding of m^{6}A, positioning FOCAS as a powerful framework for dissecting m^{6}A-mediated regulatory architectures.

Despite extensive research, m^{6}A's tumorigenic roles remain context dependent.[14–16] Inhibiting the methyltransferase METTL3 or the demethylase FTO can suppress tumor growth in acute myeloid leukemia,[64,65] underscoring the complexity of m^{6}A site-specific regulation. Precisely dissecting individual m^{6}A sites is crucial for developing RNA modification-based therapies. Although many m^{6}A peaks are universal, their functions are often cell-type-specific. Unique FiPeaks frequently derive from carRNAs, implicating ncRNAs in tumor-specific regulation and tailored therapeutic potential. Conversely, 141 universal FiGenes were enriched in transcriptional regulation with tumor-normal differential expression, suggesting their potential as pan-cancer m^{6}A biomarkers. Intriguingly, universal FiGenes exhibit high early-embryonic expression followed by rapid decline, whereas unique FiGenes progressively upregulate during differentiation with low m^{6}A conservation, further supporting tissue-specific roles. Overall, FOCAS provides valuable insights into tumor biology and opens avenues for precise, context-aware RNA modification-targeted therapies.

Limitations of the study

FOCAS captures steady-state effects of m^{6}A demethylation but lacks temporal resolution, limiting its ability to resolve dynamic processes. While it reveals shared and cell-type-specific m^{6}A regulation across cell lines, broader cancer coverage and gene-level validation are needed. FOCAS's bulk-level screening approach does not capture cell-to-cell heterogeneity in m^{6}A regulation. Future effects should extend FOCAS to diverse models, achieve single-cell resolution, and integrate machine learning frameworks to elucidate context-specific m^{6}A functions and build a mechanistic epitranscriptomic atlas, accelerating the discovery of clinical biomarkers and therapeutic targets.

RESOURCE AVAILABILITY

Lead contact

Further information and requests for resources and reagents should be directed to and will be fulfilled by the lead contact, Jun Liu (junliu1223@pku.edu.cn).

Materials availability

This study did not generate new, unique reagents.

Data and code availability

- FOCAS screen results, m^{6}A-seq, chromatin immunoprecipitation sequencing (ChIP-seq), RNA-seq, and GLORI-seq data are available in this paper's key resources table. Raw and processed datasets are deposited in the NCBI Gene Expression Omnibus (GEO) with accession

Figure 6. m^{6}A-regulated transcriptional networks affect cell fitness

(A) GO analysis of common FiGenes (n = 141, both dropout and enrich) across four cell lines using STRING (https://string-db.org).
(B) Proportion of transcription-related FiGenes among all FiGenes for each cell line.
(C) Illustration of selected transcription-associated FiGenes based on varying interaction degrees within the PPI network in Figure S6C.
(D) Correlation-matrix plot based on gene expression changes. Four modules are defined based on the Pearson correlation coefficient.
(E) Heatmap showing the DEGs (rows) versus nontarget sgRNA (Benjamini-Hochberg adjusted $p < 0.05$ and |fold change| > 1.5).
(F) H3K4me3 expression in SMMC-7721-dCas13b-*wt*FTO cells with E1 module sgRNAs versus nontarget sgRNA. Protein levels were normalized to H3 (n = 3, error bars indicate mean ± SD).
(G) H3K4me3 ChIP-seq peak numbers in two biological replicates treated with E1 module sgRNAs versus nontarget sgRNA.
(H) H3K4me3 levels around the centers of H3K4me3 ChIP-seq peaks treated with nontarget sgRNA or E1 module sgRNAs. The depicted ChIP-seq signals represent the integration of two biological replicates.
(I) Correlation of H3K4me3 changes induced by E1 module sgRNAs versus nontarget sgRNA. Pearson correlation coefficient (R) and p value are shown.
See also Figure S6.

numbers GEO: GSE302263, GSE273707, GSE301420, GSE273706, GSE273719, GSE301521, GSE301419. Other data reported in this study will be shared by the lead contact upon request.
- This paper does not report original code.
- Any additional information required to reanalyze the data reported in this paper is available from the lead contact upon request.

ACKNOWLEDGMENTS

We thank Dr. Yun Ge for valuable suggestions. We thank the National Center for Protein Sciences and the Core Facilities of Life Sciences at Peking University. This study received support from the National Key Research and Development Program of China to J.L. (2024YFA1107000 and 2023YFC3402200), the Natural Science Foundation of Beijing Municipality to J.L. (Z240010), the National Natural Science Foundation of China to J.L. (32170595), Funding by Major Program of Shenzhen Bay Laboratory to J.L. (S241101001), the Center for Life Sciences, and the School of Life Sciences of Peking University.

AUTHOR CONTRIBUTIONS

J.L. conceived the original idea and designed the original studies with help from W.W. X.Z. and X.L. performed most experiments with assistance from Y.H., Y.Q., and L.S. Y.Z. performed most bioinformatics analyses with assistance from Y.L. J.L., X.Z., Y.Z., and X.L. wrote the manuscript with help from C.L., Y.G., and J.H. and input from all authors.

DECLARATION OF INTERESTS

The authors declare no competing interests.

STAR★METHODS

Detailed methods are provided in the online version of this paper and include the following:

SUPPLEMENTAL INFORMATION

Supplemental information can be found online at https://doi.org/10.1016/j.cell.2025.11.037.

Received: August 23, 2024
Revised: August 7, 2025
Accepted: November 27, 2025

REFERENCES

1. Roundtree, I.A., Evans, M.E., Pan, T., and He, C. (2017). Dynamic RNA modifications in gene expression regulation. Cell *169*, 1187–1200. https://doi.org/10.1016/j.cell.2017.05.045.
2. Frye, M., Harada, B.T., Behm, M., and He, C. (2018). RNA modifications modulate gene expression during development. Science *361*, 1346–1349. https://doi.org/10.1126/science.aau1646.
3. Yang, L., Ma, M., Gao, Y., and Liu, J. (2025). Decoding N^6-methyladenosine's dynamic role in stem cell fate and early embryo development: insights into RNA-chromatin interactions. Curr. Opin. Genet. Dev. *91*, 102311. https://doi.org/10.1016/j.gde.2025.102311.
4. Shi, H., Wei, J., and He, C. (2019). Where, when, and how: context-dependent functions of RNA methylation writers, readers, and erasers. Mol. Cell *74*, 640–650. https://doi.org/10.1016/j.molcel.2019.04.025.
5. Zou, Z., and He, C. (2024). The YTHDF proteins display distinct cellular functions on m^{6}A-modified RNA. Trends Biochem. Sci. *49*, 611–621. https://doi.org/10.1016/j.tibs.2024.04.001.
6. Wang, X., Lu, Z., Gomez, A., Hon, G.C., Yue, Y., Han, D., Fu, Y., Parisien, M., Dai, Q., Jia, G., et al. (2014). N^6-methyladenosine-dependent regulation of messenger RNA stability. Nature *505*, 117–120. https://doi.org/10.1038/nature12730.
7. Wang, X., Zhao, B.S., Roundtree, I.A., Lu, Z., Han, D., Ma, H., Weng, X., Chen, K., Shi, H., and He, C. (2015). N^6-methyladenosine modulates messenger RNA translation efficiency. Cell *161*, 1388–1399. https://doi.org/10.1016/j.cell.2015.05.014.
8. Huang, H., Weng, H., Sun, W., Qin, X., Shi, H., Wu, H., Zhao, B.S., Mesquita, A., Liu, C., Yuan, C.L., et al. (2018). Recognition of RNA N^6-methyladenosine by IGF2BP proteins enhances mRNA stability and translation. Nat. Cell Biol. *20*, 285–295. https://doi.org/10.1038/s41556-018-0045-z.
9. Liu, J., Dou, X., Chen, C., Chen, C., Liu, C., Xu, M.M., Zhao, S., Shen, B., Gao, Y., Han, D., et al. (2020). N^6-methyladenosine of chromosome-associated regulatory RNA regulates chromatin state and transcription. Science *367*, 580–586. https://doi.org/10.1126/science.aay6018.
10. Chelmicki, T., Roger, E., Teissandier, A., Dura, M., Bonneville, L., Rucli, S., Dossin, F., Fouassier, C., Lameiras, S., and Bourc'his, D. (2021). m^{6}A RNA methylation regulates the fate of endogenous retroviruses. Nature *591*, 312–316. https://doi.org/10.1038/s41586-020-03135-1.
11. Xu, W., Li, J., He, C., Wen, J., Ma, H., Rong, B., Diao, J., Wang, L., Wang, J., Wu, F., et al. (2021). METTL3 regulates heterochromatin in mouse embryonic stem cells. Nature *591*, 317–321. https://doi.org/10.1038/s41586-021-03210-1.
12. Chen, C., Liu, W., Guo, J., Liu, Y., Liu, X., Liu, J., Dou, X., Le, R., Huang, Y., Li, C., et al. (2021). Nuclear m^{6}A reader YTHDC1 regulates the scaffold function of LINE1 RNA in mouse ESCs and early embryos. Protein Cell *12*, 455–474. https://doi.org/10.1007/s13238-021-00837-8.

13. Kang, Z., Li, R., Liu, C., Dong, X., Hu, Y., Xu, L., Liu, X., Xiang, Y., Gao, L., Si, W., et al. (2024). m^{6}A-modified cenRNA stabilizes CENPA to ensure centromere integrity in cancer cells. Cell *187*, 6035–6054.e27. https://doi.org/10.1016/j.cell.2024.08.040.

14. Deng, X., Qing, Y., Horne, D., Huang, H., and Chen, J. (2023). The roles and implications of RNA m^{6}A modification in cancer. Nat. Rev. Clin. Oncol. *20*, 507–526. https://doi.org/10.1038/s41571-023-00774-x.

15. Huang, H., Weng, H., and Chen, J. (2020). m^{6}A modification in coding and non-coding RNAs: roles and therapeutic implications in cancer. Cancer Cell *37*, 270–288. https://doi.org/10.1016/j.ccell.2020.02.004.

16. Deng, X., Su, R., Weng, H., Huang, H., Li, Z., and Chen, J. (2018). RNA N^6-methyladenosine modification in cancers: current status and perspectives. Cell Res. *28*, 507–517. https://doi.org/10.1038/s41422-018-0034-6.

17. Lan, Y., Xia, Z., Shao, Q., Lin, P., Lu, J., Xiao, X., Zheng, M., Chen, D., Dou, Y., and Xie, Q. (2025). Synonymous mutations promote tumorigenesis by disrupting m^{6}A-dependent mRNA metabolism. Cell *188*, 1828–1841.e15. https://doi.org/10.1016/j.cell.2025.01.026.

18. Liu, C., Sun, H., Yi, Y., Shen, W., Li, K., Xiao, Y., Li, F., Li, Y., Hou, Y., Lu, B., et al. (2023). Absolute quantification of single-base m^{6}A methylation in the mammalian transcriptome using GLORI. Nat. Biotechnol. *41*, 355–366. https://doi.org/10.1038/s41587-022-01487-9.

19. Xiao, Y.L., Liu, S., Ge, R., Wu, Y., He, C., Chen, M., and Tang, W. (2023). Transcriptome-wide profiling and quantification of N^6-methyladenosine by enzyme-assisted adenosine deamination. Nat. Biotechnol. *41*, 993–1003. https://doi.org/10.1038/s41587-022-01587-6.

20. Cerneckis, J., Ming, G.L., Song, H., He, C., and Shi, Y. (2024). The rise of epitranscriptomics: recent developments and future directions. Trends Pharmacol. Sci. *45*, 24–38. https://doi.org/10.1016/j.tips.2023.11.002.

21. Rauch, S., He, E., Srienc, M., Zhou, H., Zhang, Z., and Dickinson, B.C. (2019). Programmable RNA-guided RNA effector proteins built from human parts. Cell *178*, 122–134.e12. https://doi.org/10.1016/j.cell.2019.05.049.

22. Rauch, S., He, C., and Dickinson, B.C. (2018). Targeted m^{6}A reader proteins to study epitranscriptomic regulation of single RNAs. J. Am. Chem. Soc. *140*, 11974–11981. https://doi.org/10.1021/jacs.8b05012.

23. Hou, J., Zhang, H., Liu, J., Zhao, Z., Wang, J., Lu, Z., Hu, B., Zhou, J., Zhao, Z., Feng, M., et al. (2019). YTHDF2 reduction fuels inflammation and vascular abnormalization in hepatocellular carcinoma. Mol. Cancer *18*, 163. https://doi.org/10.1186/s12943-019-1082-3.

24. Xiao, Y., Wang, Y., Tang, Q., Wei, L., Zhang, X., and Jia, G. (2018). An elongation- and ligation-based qPCR amplification method for the radiolabeling-free detection of locus-specific N^6-methyladenosine modification. Angew. Chem. Int. Ed. Engl. *57*, 15995–16000. https://doi.org/10.1002/anie.201807942.

25. Sendinc, E., and Shi, Y. (2023). RNA m^{6}A methylation across the transcriptome. Mol. Cell *83*, 428–441. https://doi.org/10.1016/j.molcel.2023.01.006.

26. He, C., and Lan, F. (2021). RNA m^{6}A meets transposable elements and chromatin. Protein Cell *12*, 906–910. https://doi.org/10.1007/s13238-021-00859-2.

27. Wei, J., and He, C. (2021). Chromatin and transcriptional regulation by reversible RNA methylation. Curr. Opin. Cell Biol. *70*, 109–115. https://doi.org/10.1016/j.ceb.2020.11.005.

28. Zhu, S., Cao, Z., Liu, Z., He, Y., Wang, Y., Yuan, P., Li, W., Tian, F., Bao, Y., and Wei, W. (2019). Guide RNAs with embedded barcodes boost CRISPR-pooled screens. Genome Biol. *20*, 20. https://doi.org/10.1186/s13059-019-1628-0.

29. Xu, P., Liu, Z., Liu, Y., Ma, H., Xu, Y., Bao, Y., Zhu, S., Cao, Z., Wu, Z., Zhou, Z., et al. (2021). Genome-wide interrogation of gene functions through base editor screens empowered by barcoded sgRNAs. Nat. Biotechnol. *39*, 1403–1413. https://doi.org/10.1038/s41587-021-00944-1.

30. Li, W., Xu, H., Xiao, T., Cong, L., Love, M.I., Zhang, F., Irizarry, R.A., Liu, J.S., Brown, M., and Liu, X.S. (2014). MAGeCK enables robust identification of essential genes from genome-scale CRISPR/Cas9 knockout screens. Genome Biol. *15*, 554. https://doi.org/10.1186/s13059-014-0554-4.

31. Sondka, Z., Bamford, S., Cole, C.G., Ward, S.A., Dunham, I., and Forbes, S.A. (2018). The COSMIC cancer gene census: describing genetic dysfunction across all human cancers. Nat. Rev. Cancer *18*, 696–705. https://doi.org/10.1038/s41568-018-0060-1.

32. Tang, G., Cho, M., and Wang, X. (2022). OncoDB: an interactive online database for analysis of gene expression and viral infection in cancer. Nucleic Acids Res. *50*, D1334–D1339. https://doi.org/10.1093/nar/gkab970.

33. Tang, G., Liu, X., Cho, M., Li, Y., Tran, D.H., and Wang, X. (2024). Pan-cancer discovery of somatic mutations from RNA sequencing data. Commun. Biol. *7*, 619. https://doi.org/10.1038/s42003-024-06326-y.

34. Uhlén, M., Fagerberg, L., Hallström, B.M., Lindskog, C., Oksvold, P., Mardinoglu, A., Sivertsson, Å., Kampf, C., Sjöstedt, E., Asplund, A., et al. (2015). Proteomics. Tissue-based map of the human proteome. Science *347*, 1260419. https://doi.org/10.1126/science.1260419.

35. Ye, M., Chen, J., Yu, P., Hu, C., Wang, B., Bao, J., Lu, F., Zhong, Y., Yan, L., Kan, J., et al. (2023). WTAP activates MAPK signaling through m^{6}A methylation in VEGFA mRNA-mediated by YTHDC1 to promote colorectal cancer development. FASEB J. *37*, e23090. https://doi.org/10.1096/fj.202300344RRR.

36. Liu, X., Liu, J., Xiao, W., Zeng, Q., Bo, H., Zhu, Y., Gong, L., He, D., Xing, X., Li, R., et al. (2020). SIRT1 regulates N^6-methyladenosine RNA modification in hepatocarcinogenesis by inducing RANBP2-dependent FTO SUMOylation. Hepatology *72*, 2029–2050. https://doi.org/10.1002/hep.31222.

37. Hart, T., Chandrashekhar, M., Aregger, M., Steinhart, Z., Brown, K.R., MacLeod, G., Mis, M., Zimmermann, M., Fradet-Turcotte, A., Sun, S., et al. (2015). High-resolution CRISPR screens reveal fitness genes and genotype-specific cancer liabilities. Cell *163*, 1515–1526. https://doi.org/10.1016/j.cell.2015.11.015.

38. Luo, X., Li, H., Liang, J., Zhao, Q., Xie, Y., Ren, J., and Zuo, Z. (2021). RMVar: an updated database of functional variants involved in RNA modifications. Nucleic Acids Res. *49*, D1405–D1412. https://doi.org/10.1093/nar/gkaa811.

39. Zheng, Y., Nie, P., Peng, D., He, Z., Liu, M., Xie, Y., Miao, Y., Zuo, Z., and Ren, J. (2018). m^{6}AVar: a database of functional variants involved in m^{6}A modification. Nucleic Acids Res. *46*, D139–D145. https://doi.org/10.1093/nar/gkx895.

40. Zhang, C., Wang, X., Song, H., Yuan, J., Zhang, X., Yuan, Y., Wang, Z., Lei, Z., and He, J. (2024). m^{6}A modification-mediated LIMA1 promotes the progression of hepatocellular carcinoma through the wnt-betacatenin/Hippo pathway. Cell Biol. Toxicol. *41*, 9. https://doi.org/10.1007/s10565-024-09959-1.

41. Zhong, S., Guo, Q., Chen, X., Luo, X., Long, Y., Chong, T., Ye, M., He, H., Lu, A., Ao, K., et al. (2024). The inhibition of YTHDF3/m^{6}A/LRP6 reprograms fatty acid metabolism and suppresses lymph node metastasis in cervical cancer. Int. J. Biol. Sci. *20*, 916–936. https://doi.org/10.7150/ijbs.87203.

42. Liu, Y.Y., Xia, M., Chen, Z.B., Liao, Y.D., Zhang, C.Y., Yuan, L., Pan, Y.W., Huang, H., Lu, H.W., and Yao, S.Z. (2024). HNRNPC mediates lymphatic metastasis of cervical cancer through m^{6}A-dependent alternative splicing of FOXM1. Cell Death Dis. *15*, 732. https://doi.org/10.1038/s41419-024-07108-4.

43. Xin, T., Zhang, Z., Zhang, Y., Li, X., Wang, S., Wang, G., Li, H., Wang, B., Zhang, M., Li, W., et al. (2025). Recessive epistasis of a synonymous mutation confers cucumber domestication through epitranscriptomic regulation. Cell *188*, 4517–4529.e15. https://doi.org/10.1016/j.cell.2025.06.007.

44. Zhao, B.S., Roundtree, I.A., and He, C. (2017). Post-transcriptional gene regulation by mRNA modifications. Nat. Rev. Mol. Cell Biol. *18*, 31–42. https://doi.org/10.1038/nrm.2016.132.

45. Wang, D., Garcia-Bassets, I., Benner, C., Li, W., Su, X., Zhou, Y., Qiu, J., Liu, W., Kaikkonen, M.U., Ohgi, K.A., et al. (2011). Reprogramming transcription by distinct classes of enhancers functionally defined by eRNA. Nature *474*, 390–394. https://doi.org/10.1038/nature10006.

46. Lee, J.H., Wang, R., Xiong, F., Krakowiak, J., Liao, Z., Nguyen, P.T., Moroz-Omori, E.V., Shao, J., Zhu, X., Bolt, M.J., et al. (2021). Enhancer RNA m^{6}A methylation facilitates transcriptional condensate formation and gene activation. Mol. Cell *81*, 3368–3385.e9. https://doi.org/10.1016/j.molcel.2021.07.024.

47. Li, X., and Fu, X.D. (2019). Chromatin-associated RNAs as facilitators of functional genomic interactions. Nat. Rev. Genet. *20*, 503–519. https://doi.org/10.1038/s41576-019-0135-1.

48. Xiong, F., Wang, R., Lee, J.-H., Li, S., Chen, S.-F., Liao, Z., Hasani, L.A., Nguyen, P.T., Zhu, X., Krakowiak, J., et al. (2021). RNA m^{6}A modification orchestrates a LINE-1-host interaction that facilitates retrotransposition and contributes to long gene vulnerability. Cell Res. *31*, 861–885. https://doi.org/10.1038/s41422-021-00515-8.

49. Liu, J., Li, K., Cai, J., Zhang, M., Zhang, X., Xiong, X., Meng, H., Xu, X., Huang, Z., Peng, J., et al. (2020). Landscape and regulation of m^{6}A and m^{6}Am methylome across human and mouse tissues. Mol. Cell *77*, 426–440.e6. https://doi.org/10.1016/j.molcel.2019.09.032.

50. Li, L., Zheng, Y.L., Jiang, C., Fang, S., Zeng, T.T., Zhu, Y.H., Li, Y., Xie, D., and Guan, X.Y. (2019). HN1L-mediated transcriptional axis AP-2γ/METTL13/TCF3-ZEB1 drives tumor growth and metastasis in hepatocellular carcinoma. Cell Death Differ. *26*, 2268–2283. https://doi.org/10.1038/s41418-019-0301-1.

51. Zhao, Y.M., Jiang, Y., Wang, J.Z., Cao, S., Zhu, H., Wang, W.K., Yu, J., Liu, J., and Hui, J. (2025). GPATCH4 functions as a regulator of nucleolar R-loops in hepatocellular carcinoma cells. Nucleic Acids Res. *53*, gkaf438. https://doi.org/10.1093/nar/gkaf438.

52. Cheng, J., Zhong, Y., Chen, S., Sun, Y., Huang, L., Kang, Y., Chen, B., Chen, G., Wang, F., Tian, Y., et al. (2017). Gab2 mediates hepatocellular carcinogenesis by integrating multiple signaling pathways. FASEB J. *31*, 5530–5542. https://doi.org/10.1096/fj.201700120RR.

53. Edwards, N.J., Oberti, M., Thangudu, R.R., Cai, S., McGarvey, P.B., Jacob, S., Madhavan, S., and Ketchum, K.A. (2015). The CPTAC data portal: a resource for cancer proteomics research. J. Proteome Res. *14*, 2707–2713. https://doi.org/10.1021/pr501254j.

54. Liberzon, A., Birger, C., Thorvaldsdóttir, H., Ghandi, M., Mesirov, J.P., and Tamayo, P. (2015). The Molecular Signatures Database (MSigDB) hallmark gene set collection. Cell Syst. *1*, 417–425. https://doi.org/10.1016/j.cels.2015.12.004.

55. Bradner, J.E., Hnisz, D., and Young, R.A. (2017). Transcriptional addiction in cancer. Cell *168*, 629–643. https://doi.org/10.1016/j.cell.2016.12.013.

56. Li, R., Zhao, H., Huang, X., Zhang, J., Bai, R., Zhuang, L., Wen, S., Wu, S., Zhou, Q., Li, M., et al. (2023). Super-enhancer RNA m^{6}A promotes local chromatin accessibility and oncogene transcription in pancreatic ductal adenocarcinoma. Nat. Genet. *55*, 2224–2234. https://doi.org/10.1038/s41588-023-01568-8.

57. Dou, X., Xiao, Y., Shen, C., Wang, K., Wu, T., Liu, C., Li, Y., Yu, X., Liu, J., Dai, Q., et al. (2023). RBFOX2 recognizes N^6-methyladenosine to suppress transcription and block myeloid leukaemia differentiation. Nat. Cell Biol. *25*, 1359–1368. https://doi.org/10.1038/s41556-023-01213-w.

58. Su, Z., Zhang, Y., Tang, J., Zhou, Y., and Long, C. (2024). Multifunctional acyltransferase HBO1: a key regulatory factor for cellular functions. Cell. Mol. Biol. Lett. *29*, 141. https://doi.org/10.1186/s11658-024-00661-y.

59. Briggs, S.D., Bryk, M., Strahl, B.D., Cheung, W.L., Davie, J.K., Dent, S.Y., Winston, F., and Allis, C.D. (2001). Histone H3 lysine 4 methylation is mediated by Set1 and required for cell growth and rDNA silencing in Saccharomyces cerevisiae. Genes Dev. *15*, 3286–3295. https://doi.org/10.1101/gad.940201.

60. Wang, H., Fan, Z., Shliaha, P.V., Miele, M., Hendrickson, R.C., Jiang, X., and Helin, K. (2023). H3K4me3 regulates RNA polymerase II promoter-proximal pause-release. Nature *615*, 339–348. https://doi.org/10.1038/s41586-023-05780-8.

61. Marneros, A.G. (2020). AP-2beta/KCTD1 control distal nephron differentiation and protect against renal fibrosis. Dev. Cell *54*, 348–366.e5. https://doi.org/10.1016/j.devcel.2020.05.026.

62. Raymundo, J.R., Zhang, H., Smaldone, G., Zhu, W., Daly, K.E., Glennon, B.J., Pecoraro, G., Salvatore, M., Devine, W.A., Lo, C.W., et al. (2023). KCTD1/KCTD15 complexes control ectodermal and neural crest cell functions, and their impairment causes aplasia cutis. J. Clin. Investig. *134*, e174138. https://doi.org/10.1172/JCI174138.

63. Liang, W.W., Müller, S., Hart, S.K., Wessels, H.H., Méndez-Mancilla, A., Sookdeo, A., Choi, O., Caragine, C.M., Corman, A., Lu, L., et al. (2025). Transcriptome-scale RNA-targeting CRISPR screens reveal essential lncRNAs in human cells.. Preprint at figshare. https://doi.org/10.6084/m9.figshare.30370171.v1.

64. Yankova, E., Blackaby, W., Albertella, M., Rak, J., De Braekeleer, E., Tsagkogeorga, G., Pilka, E.S., Aspris, D., Leggate, D., Hendrick, A.G., et al. (2021). Small-molecule inhibition of METTL3 as a strategy against myeloid leukaemia. Nature *593*, 597–601. https://doi.org/10.1038/s41586-021-03536-w.

65. Huang, Y., Su, R., Sheng, Y., Dong, L., Dong, Z., Xu, H., Ni, T., Zhang, Z.S., Zhang, T., Li, C., et al. (2019). Small-molecule targeting of oncogenic FTO demethylase in acute myeloid leukemia. Cancer Cell *35*, 677–691.e10. https://doi.org/10.1016/j.ccell.2019.03.006.

66. Huang, X., Yan, J., Zhang, M., Wang, Y., Chen, Y., Fu, X., Wei, R., Zheng, X.L., Liu, Z., Zhang, X., et al. (2018). Targeting epigenetic crosstalk as a therapeutic strategy for EZH2-aberrant solid tumors. Cell *175*, 186–199.e19. https://doi.org/10.1016/j.cell.2018.08.058.

67. ENCODE Project Consortium (2012). An integrated encyclopedia of DNA elements in the human genome. Nature *489*, 57–74. https://doi.org/10.1038/nature11247.

68. Shi, Y., Fan, S., Wu, M., Zuo, Z., Li, X., Jiang, L., Shen, Q., Xu, P., Zeng, L., Zhou, Y., et al. (2019). YTHDF1 links hypoxia adaptation and non-small cell lung cancer progression. Nat. Commun. *10*, 4892. https://doi.org/10.1038/s41467-019-12801-6.

69. Martin, M. (2011). Cutadapt removes adapter sequences from high-throughput sequencing reads. EMBnet J. *17*, 10–12. https://doi.org/10.14806/ej.17.1.200.

70. Langmead, B., Trapnell, C., Pop, M., and Salzberg, S.L. (2009). Ultrafast and memory-efficient alignment of short DNA sequences to the human genome. Genome Biol. *10*, R25. https://doi.org/10.1186/gb-2009-10-3-r25.

71. Langmead, B., and Salzberg, S.L. (2012). Fast gapped-read alignment with Bowtie 2. Nat. Methods *9*, 357–359. https://doi.org/10.1038/nmeth.1923.

72. Kim, D., Paggi, J.M., Park, C., Bennett, C., and Salzberg, S.L. (2019). Graph-based genome alignment and genotyping with HISAT2 and HISAT-genotype. Nat. Biotechnol. *37*, 907–915. https://doi.org/10.1038/s41587-019-0201-4.

73. Danecek, P., Bonfield, J.K., Liddle, J., Marshall, J., Ohan, V., Pollard, M.O., Whitwham, A., Keane, T., McCarthy, S.A., Davies, R.M., et al. (2021). Twelve years of SAMtools and BCFtools. GigaScience *10*, giab008. https://doi.org/10.1093/gigascience/giab008.

74. Zhang, Y., Liu, T., Meyer, C.A., Eeckhoute, J., Johnson, D.S., Bernstein, B.E., Nusbaum, C., Myers, R.M., Brown, M., Li, W., et al. (2008). Model-based analysis of ChIP-Seq (MACS). Genome Biol. *9*, R137. https://doi.org/10.1186/gb-2008-9-9-r137.

75. Quinlan, A.R., and Hall, I.M. (2010). BEDTools: a flexible suite of utilities for comparing genomic features. Bioinformatics *26*, 841–842. https://doi.org/10.1093/bioinformatics/btq033.

76. Ramírez, F., Ryan, D.P., Grüning, B., Bhardwaj, V., Kilpert, F., Richter, A.S., Heyne, S., Dündar, F., and Manke, T. (2016). deepTools2: a next

generation web server for deep-sequencing data analysis. Nucleic Acids Res. *44*, W160–W165. https://doi.org/10.1093/nar/gkw257.

77. Heinz, S., Benner, C., Spann, N., Bertolino, E., Lin, Y.C., Laslo, P., Cheng, J.X., Murre, C., Singh, H., and Glass, C.K. (2010). Simple combinations of lineage-determining transcription factors prime cis-regulatory elements required for macrophage and B cell identities. Mol. Cell *38*, 576–589. https://doi.org/10.1016/j.molcel.2010.05.004.

78. Liao, Y., Smyth, G.K., and Shi, W. (2014). featureCounts: an efficient general purpose program for assigning sequence reads to genomic features. Bioinformatics *30*, 923–930. https://doi.org/10.1093/bioinformatics/btt656.

79. Robinson, J.T., Thorvaldsdóttir, H., Winckler, W., Guttman, M., Lander, E.S., Getz, G., and Mesirov, J.P. (2011). Integrative genomics viewer. Nat. Biotechnol. *29*, 24–26. https://doi.org/10.1038/nbt.1754.

80. Yildirim, O. (2015). Isolation of Nascent Transcripts with Click Chemistry. Curr. Protoc. Mol. Biol. *111*, 4.24.1–4.24.13. https://doi.org/10.1002/0471142727.mb0424s111.

81. Zhou, Y., Zhou, B., Pache, L., Chang, M., Khodabakhshi, A.H., Tanaseichuk, O., Benner, C., and Chanda, S.K. (2019). Metascape provides a biologist-oriented resource for the analysis of systems-level datasets. Nat. Commun. *10*, 1523. https://doi.org/10.1038/s41467-019-09234-6.

82. Sherman, B.T., Hao, M., Qiu, J., Jiao, X., Baseler, M.W., Lane, H.C., Imamichi, T., and Chang, W. (2022). DAVID a web server for functional enrichment analysis and functional annotation of gene lists (2021 update). Nucleic Acids Res. *50*, W216–W221. https://doi.org/10.1093/nar/gkac194.

83. Huang da, W., Sherman, B.T., and Lempicki, R.A. (2009). Systematic and integrative analysis of large gene lists using DAVID bioinformatics resources. Nat. Protoc. *4*, 44–57. https://doi.org/10.1038/nprot.2008.211.

Please cite this article in press as: Zhang et al., FOCAS: Transcriptome-wide screening of individual m^{6}A sites functionally dissects epitranscriptomic control of gene expression in cancer, Cell (2026), https://doi.org/10.1016/j.cell.2025.11.037

STAR★METHODS

KEY RESOURCES TABLE

REAGENT or RESOURCE	SOURCE	IDENTIFIER
Antibodies		
Rabbit monoclonal anti-N^6-methyladenosine	New England Biolabs	Cat# E1610S; RRID: AB_2923416
Mouse monoclonal anti-GAPDH	Proteintech	Cat# HRP-60004; RRID: AB_2737588
Rabbit polyclonal anti-H3	Abcam	Cat# ab1791; RRID: AB_302613
Rabbit polyclonal anti-SNRP70	Abcam	Cat# ab83306; RRID: AB_10673827
Rabbit polyclonal anti-GNAO1	ABclonal	Cat# A2510; RRID:AB_2764401
Rabbit polyclonal anti-LIMA1	ABclonal	Cat# A11682; RRID:AB_2758685
Mouse polyclonal anti-LRP6	MedChemExpress	Cat# HY-P80212; RRID:AB_3102859
Rabbit polyclonal anti-FOXM1	Beyotime	Cat# AF6924; RRID:AB_3698663
Rabbit monoclonal anti-YTHDF2	Abcam	Cat# ab246514; RRID:AB_2891213
Rabbit monoclonal anti-YTHDC1	Abcam	Cat# ab220159; RRID:AB_2923059
Rabbit polyclonal anti-IGF2BP2	Proteintech	Cat# 11601-1-AP; RRID:AB_2122672
Rabbit polyclonal anti-SAFB	Proteintech	Cat# 21857-1-AP; RRID:AB_2878928
Rabbit polyclonal anti-histone H3 (trimethyl K4)	Abcam	Cat# ab8580; RRID:AB_306649
Rabbit polyclonal anti-KCTD1	Bioss	Cat# bs-16924R; RRID:AB_3095546
Rabbit polyclonal anti-CPSF3L (INTS11)	ABclonal	Cat# A6566; RRID:AB_2767160
Rabbit polyclonal anti-SETD1B	ABclonal	Cat# A20155; RRID:AB_2862942
Goat anti-rabbit IgG, HRP-linked antibody	Cell Signaling Technology	Cat# 7074; RRID:AB_2099233
Goat anti-mouse IgG, HRP-linked antibody	Cell Signaling Technology	Cat# 7076; RRID:AB_330924
Bacterial and virus strains		
DH5α competent cell	Sangon Biotech	Cat# B528413
*Trans*5α chemically competent cell	Transgen	Cat# CD201-01
TransDB3.1 chemically competent cell	Transgen	Cat# CD531-01
E. coli HST08 premium electro-cells	TaKaRa	Cat# 9028
Chemicals, peptides, and recombinant proteins		
DMEM	GIBCO	Cat# 11965
Fetal bovine serum	Gemini	Cat# 900-108
L-Glutamine	Meilunbio	Cat# MA0155
Trypsin-EDTA	GIBCO	Cat# 15400054
Opti-MEM I reduced serum medium	GIBCO	Cat# 31985070
Lipofectamine 2000 reagent	Thermo Fisher Scientific	Cat# 11668019
Bovine serum albumin	Sigma-Aldrich	Cat# B2064
Dimethyl sulfoxide	Sigma-Aldrich	Cat# D2650
TRIzol reagent	Invitrogen	Cat# 15596026
RNA isolator total RNA extraction reagent	Vazyme	Cat# R401-01
Actinomycin D	MedChemExpress	Cat# HY-17559
Gibson assembly master mix	New England Biolabs	Cat# E2611
T4 DNA ligase	New England Biolabs	Cat# M0202
Tirchloromethane	TGREAG	Cat# 112049
Isopropyl alcohol	TGREAG	Cat# 106030
Ethanol	Concord	Cat# 8009LC0500
Methanol	TGREAG	Cat# 104028
GlycoBlue Coprecipitant (15 mg/mL)	Invitrogen	Cat# AM9516

(*Continued on next page*)

Please cite this article in press as: Zhang et al., FOCAS: Transcriptome-wide screening of individual m^{6}A sites functionally dissects epitranscriptomic control of gene expression in cancer, Cell (2026), https://doi.org/10.1016/j.cell.2025.11.037

Continued

REAGENT or RESOURCE	SOURCE	IDENTIFIER
DTT	Yuanye	Cat# S11080
Sodium deoxycholate	Sigma-Aldrich	Cat# D6750
Pierce high-sensitivity streptavidin-HRP	Thermo Fisher Scientific	Cat # 21130
Protease inhibitor cocktail	Sigma	Cat# P8849
Puromycin	Beyotime	Cat# ST551
Polybrene	Solarbio	Cat# H8761
Pierce Protein G magnetic beads	Thermo Fisher Scientific	Cat# 88848
Pierce Protein A magnetic beads	Thermo Fisher Scientific	Cat# 88846
AMPure XP	BECKMAN	Cat# A63881
DNA clean beads	Vazyme	Cat# N411-02
Dynabeads MyOne Streptavidin C1	Invitrogen	Cat# 65002
Dynabeads Oligo $(dT)_{25}$	Invitrogen	Cat# 61002
Glycerol	ABCONE	Cat# G46055
HEPES	ABCONE	Cat# H33755
Tween 20	ABCONE	Cat# P87875
Triton X-100	Sigma	Cat# X100-500ML
Agarose	ABCONE	Cat# A47902
Ampicillin	Sangon biotech	Cat# B541011
PMSF	Solarbio	Cat# P0100
Proteinase K	Invitrogen	Cat# 25530015
DNase I	New England Biolabs	Cat# M0303
RNase T1	Thermo Fisher Scientific	Cat# EN0541
RiboLock RNase inhibitor	Thermo Fisher Scientific	Cat# EO0384
UltraPure DNase/RNase-free distilled water	Invitrogen	Cat# 10977015
RLT buffer	Qiagen	Cat# 79216
Esp3I	New England Biolabs	Cat# R0734L
Acetonitrile	Concord	Cat# 8002LC0500
Bst 2.0 DNA polymerase	New England Biolabs	Cat# M0537
SplintR ligase	New England Biolabs	Cat# M0375
Deoxynucleotide (dNTP) solution mix	New England Biolabs	Cat# N0447
Adenosine 5′-triphosphate (ATP)	New England Biolabs	Cat# P0756
Nuclease P1	Fujifilm Wako	Cat# 145-08221
PEG 8000	Solarbio	Cat# P8260
4% Paraformaldehyde fix solution (PFA)	BBI	Cat# E672002-0100
0.1% Crystal violet	Solarbio	Cat# G1063
RIPA buffer (high)	Solarbio	Cat# R0010
Immobilon-P Membrane, PVDF, 0.45 μm	Millipore	Cat# IPVH00010
FGSuper sensitive ECL luminescence reagent	Meilunbio	Cat# MA0186-2
Sodium L-ascorbate	Mei5bio	Cat# S60320
PMDTA	Sigma-Aldrich	Cat# 369497
Biotin azide	Ribobio	Cat# C00101
NEBNext® Magnesium RNA Fragmentation Module	New England Biolabs	Cat# E6150S
Glyoxal solution (8.8 M in H_2O)	Sigma-Aldrich	Cat# 50649
Sodium Nitrite	Sigma-Aldrich	Cat# 3143-100g
Boric acid	Sigma-Aldrich	Cat# B0394

(*Continued on next page*)

Please cite this article in press as: Zhang et al., FOCAS: Transcriptome-wide screening of individual m^{6}A sites functionally dissects epitranscriptomic control of gene expression in cancer, Cell (2026), https://doi.org/10.1016/j.cell.2025.11.037

Continued

REAGENT or RESOURCE	SOURCE	IDENTIFIER
Critical commercial assays		
DNA Clean & Concentrator Kits	Zymo	Cat# DP4033
RNA Clean & Concentrator Kits	Zymo	Cat# R1017
DNeasy Blood and Tissue Kit	Qiagen	Cat# 69506
NEBNext® Q5® Hot Start HiFi PCR Master Mix	New England Biolabs	Cat# M0543S
NEBNext Ultra II Q5 Master Mix	New England Biolabs	Cat# M0544
Taq Pro Universal SYBR qPCR Master Mix	Vazyme	Cat# Q712-02
Pierce BCA Protein Assay Kit	Thermo Fisher Scientific	Cat# 23225
VAHTS Stranded mRNA-seq Library Prep Kits	Vazyme	Cat# NR602
AccuNext Stranded RNA-seq Library Kit for Illumina	Accurate Biology	Cat# AG12504
Ribo-off Globin & rRNA Depletion Kit (Human/Mouse/Rat)	Vazyme	Cat# N408
RiboMinus™ Eukaryote Kit v2	Invitrogen	Cat# A15020
Clonech SMARTer Stranded Total RNA-Seq Kit v2 - Pico Input Mammalian	Takara	Cat# 634413
Clonech SMARTer Stranded Total RNA-Seq Kit v3 - Pico Input Mammalian	Takara	Cat# 634487
VAHTS Universal Pro DNA Library Prep Kit for Illumina	Vazyme	Cat# N608
Deposited data		
CRISPR dCas13b-FTO screening	This study	GEO: GSE302263
caRNA m^{6}A-seq in SMMC-7721 cells	This study	GEO: GSE273707
caRNA m^{6}A-seq in HepG2 cells	This study	GEO: GSE301420
caRNA m^{6}A-seq in HCT116 cells	This study	GEO: GSE301420
caRNA m^{6}A-seq in HeLa cells	This study	GEO: GSE301420
Total RNA m^{6}A-seq in HepG2 cells	This study	GEO: GSE301420
Total RNA m^{6}A-seq in HCT116 cells	This study	GEO: GSE301420
Total RNA m^{6}A-seq in HeLa cells	This study	GEO: GSE301420
caRNA m^{6}A-seq in RKO cells	This study	Unpublished
Total RNA m^{6}A-seq in RKO cells	This study	Unpublished
caRNA m^{6}A-seq in MDA-MB-231 cells	This study	Unpublished
caRNA m^{6}A-seq in A375 cells	This study	Unpublished
Total RNA m^{6}A-seq in A375 cells	This study	Unpublished
caRNA m^{6}A-seq in H1299 cells	This study	Unpublished
Total RNA m^{6}A-seq in H1299 cells	This study	Unpublished
H3K4me3 ChIP-seq in SMMC-7721 cells	This study	GEO: GSE273706
RNA-seq in SMMC-7721 cells	This study	GEO: GSE273719, GSE301521
RNA-seq in HepG2 cells	This study	GEO: GSE301521
RNA-seq in HCT116 cells	This study	GEO: GSE301521
RNA-seq in HeLa cells	This study	GEO: GSE301521
GLORI-seq in SMMC-7721 cells	This study	GEO: GSE301419
GLORI-seq in HepG2 cells	This study	GEO: GSE301419
GLORI-seq in HCT116 cells	This study	GEO: GSE301419
GLORI-seq in HeLa cells	This study	GEO: GSE301419
H3K27ac ChIP-seq in SMMC-7721 cells	Huang et al.[66]	GEO: GSE119086
H3K27ac ChIP-seq in HepG2 cells	Dunham et al.[67]	GEO: GSE29611
H3K27ac ChIP-seq in HCT116 cells	Dunham et al.[67]	GEO: GSE96299

(*Continued on next page*)

Please cite this article in press as: Zhang et al., FOCAS: Transcriptome-wide screening of individual m^{6}A sites functionally dissects epitranscriptomic control of gene expression in cancer, Cell (2026), https://doi.org/10.1016/j.cell.2025.11.037

Continued

REAGENT or RESOURCE	SOURCE	IDENTIFIER
H3K27ac ChIP-seq in HeLa cells	Dunham et al.[67]	GEO: GSE29611
caRNA m^{6}A-seq in HepG2 cells	Dou et al.[57]	GEO: GSE205709
caRNA m^{6}A-seq in K562 cells	Dou et al.[57]	GEO: GSE205709
Total RNA m^{6}A-seq in A549 cells	Shi et al.[68]	GEO: GSE136433
Total RNA m^{6}A-seq in SMMC-7721 cells	Hou et al.[23]	GEO: GSE120860
Experimental models: Cell lines		
HEK293T	N/A	N/A
SMMC-7721	N/A	N/A
SMMC-7721-dCas13b-*wt*FTO-sc	N/A	N/A
SMMC-7721-dCas13b-*mut*FTO-sc	N/A	N/A
HepG2	N/A	N/A
HepG2-dCas13b-*wt*FTO-sc	N/A	N/A
HepG2-dCas13b-*mut*FTO-sc	N/A	N/A
HCT116	N/A	N/A
HCT116-dCas13b-*wt*FTO-sc	N/A	N/A
HCT116-dCas13b-*mut*FTO-sc	N/A	N/A
HeLa	N/A	N/A
HeLa-dCas13b-*wt*FTO-sc	N/A	N/A
HeLa-dCas13b-*mut*FTO-sc	N/A	N/A
Oligonucleotides		
Oligonucleotides are listed in Table S1	Twist Bioscience, Generay Biotechnology, Ruibiotech	Table S1
Recombinant DNA		
pLenti-PspCas13b-*wt*FTO-mCherry	This study	N/A
pLenti-PspCas13b-*mut*FTO-mCherry	This study	N/A
pVSV-G	A gift from W. Wei's laboratory (Peking University)	N/A
pR8.74	A gift from W. Wei's laboratory (Peking University)	N/A
pLKO.1-TRC vector	N/A	N/A
pLKO.1-shKCTD1 vector	This paper	N/A
pCG-2.0-PspCas13b-SV40-Puro-iBAR-1	This study	N/A
pCG-2.0-PspCas13b-SV40-Puro-iBAR-2	This study	N/A
pCG-2.0-PspCas13b-SV40-Puro-iBAR-3	This study	N/A
LentiCRISPRv2-KOGNAO1-1	This study	N/A
LentiCRISPRv2-KOGNAO1-2	This study	N/A
LentiCRISPRv2-KOGNAO1-3	This study	N/A
LentiCRISPRv2-KOLIMA1-1	This study	N/A
LentiCRISPRv2-KOLIMA1-2	This study	N/A
LentiCRISPRv2-KOLIMA1-3	This study	N/A
LentiCRISPRv2-KOLRP6-1	This study	N/A
LentiCRISPRv2-KOLRP6-2	This study	N/A
LentiCRISPRv2-KOLRP6-3	This study	N/A
LentiCRISPRv2-KOFOXM1-1	This study	N/A
LentiCRISPRv2-KOFOXM1-2	This study	N/A
LentiCRISPRv2-KOFOXM1-3	This study	N/A
pcDNA 3.0-EV	This study	N/A
pcDNA 3.0-*wt*GNAO1	This study	N/A

(*Continued on next page*)

Please cite this article in press as: Zhang et al., FOCAS: Transcriptome-wide screening of individual m^{6}A sites functionally dissects epitranscriptomic control of gene expression in cancer, Cell (2026), https://doi.org/10.1016/j.cell.2025.11.037

Continued

REAGENT or RESOURCE	SOURCE	IDENTIFIER
pcDNA 3.0-*mut*GNAO1-c.A2472C	This study	N/A
pcDNA 3.0-*mut*GNAO1-c.A2472G	This study	N/A
pcDNA 3.0-*mut*GNAO1-c.A2472T	This study	N/A
pcDNA 3.0-*wt*LIMA1	This study	N/A
pcDNA 3.0-*mut*LIMA1-c.A387C	This study	N/A
pcDNA 3.0-*mut*LIMA1-c.A387G	This study	N/A
pcDNA 3.0-*mut*LIMA1-c.A387T	This study	N/A
pcDNA 3.0-*wt*LRP6	This study	N/A
pcDNA 3.0-*mut*LRP6-c.A556C	This study	N/A
pcDNA 3.0-*mut*LRP6-c.A556G	This study	N/A
pcDNA 3.0-*mut*LRP6-c.A556T	This study	N/A
pcDNA 3.0-*wt*FOXM1	This study	N/A
pcDNA 3.0-*mut*FOXM1-c.A3329C	This study	N/A
pcDNA 3.0-*mut*FOXM1-c.A3329G	This study	N/A
pcDNA 3.0-*mut*FOXM1-c.A3329T	This study	N/A
plx-KCTD1-puromycin	This study	N/A
Software and algorithms		
Prism 9	GraphPad	https://www.graphpad.com
Fiji/ImageJ	National Institutes of Health	https://imagej.net/Fiji
Cytoscape v3.9.1	Cytoscape	https://cytoscape.org/
FastQC v0.11.9	Babraham Bioinformatics	https://www.bioinformatics.babraham.ac.uk/projects/fastqc/
Trim Galore! v0.6.7	Martin[69]	https://www.bioinformatics.babraham.ac.uk/projects/trim_galore/
Bowtie v1.0.0	Langmead and Salzberg[70]	https://bowtie-bio.sourceforge.net/index.shtml
Bowtie2 v2.2.5	Langmead and Salzberg[71]	http://bowtie-bio.sourceforge.net/bowtie2/index.shtml
HISAT2 v2.2.1	Kim et al.[72]	https://ccb.jhu.edu/software/hisat2/index.shtml
samtools v1.10	Danecek et al.[73]	http://samtools.sourceforge.net/
macs2 v2.2.7.1	Zhang et al.[74]	https://github.com/macs3-project/MACS/wiki/Install-macs2
bedtools v2.26.0	Quinlan and Hall[75]	https://bedtools.readthedocs.io/en/latest/
Deeptools v3.5.1	Ramirez et al.[76]	https://deeptools.readthedocs.io/en/develop/index.html
Homer v4.11	Heinz et al.[77]	http://homer.ucsd.edu/homer/
FeatureCounts v2.0.1	Liao et al.[78]	https://subread.sourceforge.net/
picard toolkit v2.26.0	Broad Institute	http://broadinstitute.github.io/picard/
IGV v2.15.4	Robinson et al.[79]	http://software.broadinstitute.org/software/igv/
R v4.3.2	R	https://www.r-project.org/

EXPERIMENTAL MODEL AND STUDY PARTICIPANT DETAILS

Cell culture

SMMC-7721 (male), HepG2 (male), HCT116 (male), HeLa (female) and HEK293T cells (female) were cultured in DMEM (Gibco, 11965) supplemented with 10% fetal bovine serum (FBS; Gemini, 900-108) and 1% glutamine (Meilunbio, MA0155) at 37°C with 5% CO_2. To establish the SMMC-7721-dPspCas13b-*wt*/*mut*FTO-mCherry, HepG2-dPspCas13b-*wt*/*mut*FTO-mCherry, HCT116-dPspCas13b-*wt*/*mut*FTO-mCherry and HeLa-dPspCas13b-*wt*/*mut*FTO-mCherry stable cell lines, lentivirus was produced by transfecting

HEK293T cells with pLenti-dPspCas13b-*wt*/*mut*FTO-mCherry and lentiviral packaging plasmids pVSV-G and pR8.74. After 48 h of transfection, single clones were isolated using fluorescence-activated cell sorting (BD Aria Fusion) and maintained in culture until reaching sufficient cell numbers.

METHOD DETAILS

Plasmid construction

pLenti-dPspCas13b-*wt*/*mut*FTO-mCherry plasmids were used for packaging lentivirus expressing either dPspCas13b-*wt*FTO or dPspCas13b-*mut*FTO (nuclease-inactive). sgRNA plasmids used for individual validation were generated by inserting spacer sequences into the pCG-2.0-dPspCas13b-SV40-Puro vector via Golden Gate assembly. sgRNA plasmids designed for the knockout of *GNAO1*, *LIMA1*, *LRP6*, and *FOXM1* were constructed by inserting sgRNA sequences into the LentiCRISPRv2 vector via Gibson assembly (New England Biolabs). Human protein-coding sequences of *KCTD1*, *LIMA1*, and *LRP6* were inserted into the plx304-puromycin plasmid or pcDNA3.0 plasmid via Gibson assembly. Human full-length sequences of *GNAO1* and *FOXM1* were inserted into the pcDNA3.0 plasmid via Gibson assembly. *KCTD1* short hairpin RNA (shRNA) plasmid was from MISSION LentiPlex Human Pooled shRNA Library TRC1.0 (Merk, SHPH1). sgRNA and shRNA sequences are listed in Table S1.

sgRNA library design

The human genome reference sequences and gene annotations were obtained from UCSC (GRCh38/hg38). sgRNA libraries for FOCAS were designed as follows:

(1) Sequences within common m^{6}A peaks detected in two replicates for each cell line were captured using the BSgenome package (v1.70.1), and only the strand complementary to the m^{6}A peak was retained.
(2) The complementary sequence of the motif along the peak sequence obtained above was searched, and the 100 nucleotides upstream of the first motif to 100 nucleotides downstream of the last motif were used as the candidate range for sgRNA design.
(3) Within the range of candidate sgRNA design, 30-nucleotide fragments were extracted at 35-nucleotide intervals to create the initial sgRNA library.
(4) To ensure optimal sgRNA on-targeting efficiency, we excluded the aforementioned sgRNAs that fulfilled any of the following criteria: (1) exhibit matches with multiple regions in the human genome, allowing for 1-bp mismatch, using bowtie (v1.0.0)[70] with the parameter "-k 2 -v 1"; (2) contain polyT sequences; (3) have a GC content lower than 0.2 or higher than 0.8; and (4) contain self-complementary sequences longer than 10 nucleotides.
(5) sgRNAs designed from total RNA m^{6}A-seq-derived peaks were retained only if they were located in exon regions.

Library production

The oligonucleotide pool was synthesized by Twist Bioscience. sgRNA sequences were amplified by PCR using primers targeting the flanking sequences of the oligonucleotides (see Table S1). Subsequently, the sgRNA sequences were inserted into three types of pCG-2.0-PspCas13b-SV40-Puro-iBAR vectors via Golden Gate assembly. The following three validated iBARs were incorporated into this library: AGCGAG, CAGTGC, and AGTGGA (5′–3′). After purification of the Golden Gate products by DNA Clean & Concentrator-5 kit (Zymo), the sgRNAs with iBARs were electroporated into competent cells (TaKaRa) to generate the plasmid library. This plasmid library was then co-transfected into HEK293T cells along with lentiviral packaging plasmids pVSV-G and pR8.74 using Lipofectamine 2000 Reagent DNA transfection reagent to produce the lentiviral library, which was collected 48 h after transfection. For lentivirus library titration, SMMC-7721, HepG2, HCT116 and HeLa cells were seeded into six-well plates and infected with lentiviruses at volumes ranging from 0 to 32 μL. After 48 h of infection, the SMMC-7721, HepG2, HCT116 and HeLa cells were replated and cultured with or without 2 μg/μL puromycin for an additional 48 h. Viable cells in each group were enumerated, and virus titer was calculated based on cell viability ratios.

Functional m^{6}A site screening in four cancer cell lines

Four kinds of dPspCas13b-*wt*FTO or dPspCas13b-*mut*FTO expressing cell lines were exposed to the lentiviral library at a high MOI of 3. Forty-eight hours after infection, cells were treated with 2 μg/μL puromycin for 48 h. A subset of viable cells was collected as the reference group, marking this time point as 0 doubling time (D_t, 41 h for SMMC-7721, 36 h for HepG2, 22 h for HCT116, and 36 h for HeLa). The remaining library cells were cultured and maintained at a 500-fold coverage for fitness screening. Passage of library cells occurred every 3 days, and cells were collected as the experimental group on 14 D_t. Genomic DNA was isolated from cell pellets of both the reference and experimental groups using a DNeasy Blood and Tissue Kit (Qiagen). The sgRNA sequences integrated into the cellular genome were amplified by PCR using a NEBNext® Q5® Hot Start HiFi PCR Master Mix (New England Biolabs) with five pairs of primers (refer to Table S1). The following PCR conditions were used: initial denaturation at 95°C for 30 s; 26 cycles of denaturation at 95°C for 10 s, annealing at 60°C for 30 s, and extension at 72°C for 15 s; and a final extension at 72°C for 15 s. The PCR products were purified using a DNA Clean & Concentrator-5 kit (Zymo) and subsequently subjected to NGS analysis. Quality control was

Please cite this article in press as: Zhang et al., FOCAS: Transcriptome-wide screening of individual m^{6}A sites functionally dissects epitranscriptomic control of gene expression in cancer, Cell (2026), https://doi.org/10.1016/j.cell.2025.11.037

performed on all sequenced libraries using FastQC (v0.11.9; https://www.bioinformatics.babraham.ac.uk/projects/fastqc). sgRNA read counts were obtained using MAGeCK (v0.5.9.5) running on Linux. For each sample, read counts from two biological replicates were averaged to generate the final input for downstream analysis. The dCas13b-*mut*FTO samples were used as catalytically inactive controls for normalization. For each cell line, the fold change in sgRNA abundance between 0 D_t and 14 D_t in the *mut*FTO background was calculated to derive a guide-specific scale factor. These scale factors were then applied to normalize the corresponding wild-type 14 D_t counts, correcting for guide-specific variability and nonspecific effects. Significant sgRNAs were identified using the MAGeCK test module, with an FDR threshold of 0.05 applied independently in each cell line.

Cell fractionation

Cells were fractionated according to a previously published procedure.[9] Briefly, 5×10^6 to 1×10^7 cells were collected and washed with 1 mL of cold 1× PBS/1 mM EDTA buffer. The cell pellet was collected by centrifugation at 500 *g* at room temperature. Next, 200 μL of ice-cold lysis buffer (10 mM Tris-HCl, pH 7.5, 0.1% NP-40, and 150 mM NaCl) was added, and the cell pellet was gently flicked to mix and incubated on ice for 5 min. The cell lysate was then gently pipetted over equal volumes of chilled sucrose cushion (24% RNase-free sucrose in lysis buffer) and centrifuged at 15,000 *g* for 10 min at 4°C. The supernatant was collected as the cytoplasmic fraction. Next, 200 μL of ice-cold 1× PBS/1 mM EDTA was gently added to the nuclear pellet (without dislodging it) and aspirated. The pellet was then resuspended in 100 μL of prechilled glycerol buffer (20 mM Tris-HCl, pH 7.9, 75 mM NaCl, 0.5 mM EDTA, 0.85 mM DTT, 0.125 mM PMSF, and 50% glycerol) with gentle flicking of the tube. A double volume of cold nuclei lysis buffer (10 mM HEPES, pH 7.6, 1 mM DTT, 7.5 mM $MgCl_2$, 0.2 mM EDTA, 0.3 M NaCl, and 3 M urea) was added, and the mixture was vortexed vigorously four times for 5 s each. The nuclei pellet mixtures were incubated on ice for 2 min and centrifuged at 15,000 *g* for 2 min at 4°C. The supernatant was collected as the nucleoplasm fraction, and the pellet was gently rinsed with cold 1× PBS/1 mM EDTA (without dislodging) and collected as the chromosome-associated fraction. The chromatin-associated fraction was then lysed using TRIzol reagent (Invitrogen), followed by caRNA extraction. The corresponding protein lysates from the cytoplasmic, nucleoplasmic, and chromatin-associated fractions were mixed with 6 × protein loading buffer (TransGen) and boiled at 98°C for 10 minutes. Protein samples from each fraction were collected, and the efficiency of cellular fractionation could be subsequently verified by western bloting.

RNA isolation

After cell collection, TRIzol reagent (Invitrogen) or RNA isolator total RNA extraction reagent (Vazyme) was used to extract total RNA following the manufacturer's instructions. To isolate mRNA and non-rRNA from total RNA or caRNA, a Dynabeads mRNA Purification Kit (Invitrogen) and RiboMinus transcriptome isolation kit (Invitrogen) were used individually following the manufacturer's protocols. A Nanodrop (Invitrogen) was used to determine RNA concentration, measuring the UV absorbance at 260 nm.

RT-qPCR

RT-qPCR was used to evaluate the relative abundance of RNA. Total RNA or caRNA was reverse transcribed into cDNA using HiScript III RT SuperMix (Vazyme). *GAPDH*, histone H3, or the m^{6}A spike-in from the EpiMark *N*^{6}-Methyladenosine Enrichment Kit (New England Biolabs) served an internal control. qPCR was performed on a LightCycler 480 II system (Roche) using Taq Pro Universal SYBR qPCR Master Mix (Vazyme). Primer sequences are listed in Table S1. Relative changes in expression were calculated using the $\Delta\Delta C_t$ method.

Western blotting

Cells were collected and lysed with RIPA buffer (Solarbio) containing 1% PMSF (Solarbio) on ice for 30 min, and protein concentration was measured using a BCA kit (Thermo) following the manufacturer's protocol. Lysates were mixed with 6 × loading buffer (TransGen), boiled at 98°C for 10 min, and stored at −80°C for later use. A total of 10 μg of protein per sample was loaded into a 12% SDS-PAGE gel and transferred to a PVDF membrane (Millipore, IPVH00010). Membranes were blocked in 5% milk TBST at room temperature for 60 min, incubated overnight at 4°C with a diluted primary antibody solution, and washed and incubated in a dilution of secondary antibody conjugated to horseradish peroxidase (HRP) at room temperature for 2 h. The prepared ECL (Meilunbio) working liquid was added and incubated at room temperature for 1–2 min. Protein bands were visualized using a CCD camera (Tanon).

m^{6}A-IP and RT-qPCR quantification of RNA methylation

To quantify changes in m^{6}A methylation of specific target genes, we conducted m^{6}A-IP enrichment followed by RT-qPCR. Briefly, 1 μL of 1:1000 diluted m^{6}A and non-m^{6}A spike-in from the EpiMark *N*^{6}-Methyladenosine Enrichment Kit (New England Biolabs) was added to 100 ng of mRNA or nonribosomal caRNA extracted from cells. m^{6}A-IP was performed using an EpiMark *N*^{6}-Methyladenosine Enrichment Kit, as per the manufacturer's protocols. Briefly, the purified RNA was incubated with Protein A/G magnetic beads (Invitrogen) conjugated to an anti-m^{6}A antibody in m^{6}A reaction buffer (150 mM NaCl, 10 mM Tris-HCl pH7.5, 0.1% NP40) with 1 U/mL RiboLock RNase inhibitor (Invitrogen) for 2 hours at 4°C with gentle rotation. Following the incubation, the bead-RNA complexes were washed stringently with low-salt reaction buffer (50 mM NaCl, 10 mM Tris-HCl pH7.5, 0.1% NP40) and high-salt reaction buffer (500 mM NaCl, 10 mM Tris-HCl pH7.5, 0.1% NP40) to remove non-specifically bound RNA. The bound m^{6}A-modified

Please cite this article in press as: Zhang et al., FOCAS: Transcriptome-wide screening of individual m^{6}A sites functionally dissects epitranscriptomic control of gene expression in cancer, Cell (2026), https://doi.org/10.1016/j.cell.2025.11.037

RNA was finally eluted from the beads using RLT buffer (Qiagen).The resulting purified RNA samples were used as templates for RT-qPCR, with the spike-in serving as internal normalization controls. For carRNA detection, nonribosomal caRNA was extracted and primers were designed near the m^{6}A-modified sites. For mRNA detection, polyA-enriched RNA was used, and primers were designed within exonic regions. m^{6}A levels detection on mRNA-derived and carRNA-derived transcripts was performed using primers specifically targeting either mRNA or carRNA.

SELECT

Identification of specific m^{6}A sites on RNA was performed using a previously established procedure.[24] Briefly, 1.5 μg of total RNA was combined with 100 nM up primer, 100 nM down primer, and 5 μM dNTP in 17 μL of 1× CutSmart buffer (New England Biolabs). The RNA and primers were annealed using the following temperature gradient process: 90°C for 1 min, 80°C for 1 min, 70°C for 1 min, 60°C for 1 min, 50°C for 1 min, 40°C for 1 min, 30°C for 1 min, 20°C for 1 min, 1°C for 1 min, and hold at 4°C. Next, a 3 μL mixture containing 0.01 U of Bst DNA polymerase, 0.5 U of SplintR ligase, and 10 nmol ATP was added to the previous mixture, resulting in a final volume of 20 μL. The reaction mixture was incubated at 40°C for 20 min, denatured at 80°C for 20 min, and maintained at 4°C. Subsequently, RT-qPCR was performed on a LightCycler 480 II system (Roche) using Taq Pro Universal SYBR qPCR Master Mix (Vazyme). All SELECT experiments were conducted with treatment and control groups processed in parallel within the same experimental batch.

LC-MS/MS quantification of m^{6}A methylation

Non-ribosomal RNA or mRNA (20 ng) was digested with nuclease P1 (Wako) in 17 μL of buffer containing 10 mM NH_4Ac (pH 5.3) at 42°C for 2 h. rSAP enzyme (1 U; New England Biolabs) and 2 μL of 10 × rCutsmart buffer (New England Biolabs) were added and incubated at 37°C for 6 h or overnight. The digested sample was centrifuged at 13,000 rpm for 10 min at 4°C, and 5 μL of the supernatant was injected into the LC-MS/MS. Nucleosides were separated by reverse ultraperformance liquid chromatography on a C18 column and detected by a triple-quadrupole mass spectrometer (AB SCIEX QTRAP 6500) in positive ion multiple reaction-monitoring mode. The nucleosides were quantified by retention time and nucleoside-to-base ion mass transitions (268 to 136 for A and 282 to 150 for m^{6}A). Quantification was performed by comparison with standard curves obtained from pure nucleoside standards from the same batch of samples. The m^{6}A level was calculated as the ratio of m^{6}A to the average of A, U, C, and G, according to the calibration concentration.

GLORI library construction

mRNA was fragmented by incubation at 94°C for 3 min in fragment buffer (New England Biolabs). After terminating the fragmentation reaction, the mRNA was purified by ethanol precipitation. To 7 μL of the purified RNA, 3 μL of glyoxal solution (8.8 M in H_2O, Sigma-Aldrich) and 10 μL of DMSO were added. The mixture was incubated at 37°C for 30 min in a preheated thermocycler. After incubation, the tubes were placed on ice, followed by the addition of 7.5 μL 5 M $NaNO_2$ (Sigma-Aldrich), 4 μL 500 mM MES (pH 6.0), 5 μL glyoxal solution (8.8 M in H_2O, Sigma-Aldrich), 5 μL saturated H_3BO_3 solution (Sigma-Aldrich) and 8.5 μL nuclease-free water. The reaction was then incubated at 50°C for 30 min. RNA was purified by ethanol precipitation. The RNA pellets were dissolved in 25 μL deprotection buffer, prepared by mixing 10 mL of 1 M triethylammonium acetate solution (pH 8.6) with 9.5 mL of deionized formamide and adjusting the volume to 20 mL with nuclease-free water. The mixture was incubated at 95°C for 10 min. RNA was purified by ethanol precipitation. Library preparation was then performed using SMARTer Stranded Total RNA-Seq kits v3 Pico Input mammalian (Takara).

GLORI-seq analysis

Reads R2 from Illumina sequencing reads were firstly trimmed by Trim Galore (v0.6.7)[69] to remove adapters and low-quality bases with command as follows: "trim_galore -q 20 –stringency 1 -e 0.3 –length 35". Seqkit (v.2.8.2) was then used to deduplicate PCR based on the 10-base-pair UMI at the 5' end of reads R2 with parameters as follows: "seqkit rmdup -s". Finally, FASTX-Toolkit (v.0.0.14) was used to remove UMI in the deduplication reads with parameters as follows: "fastx_trimmer -f 15". For the downstream analysis we used GLORI-tools (https://github.com/liucongcas/GLORI-tools) with default parameters.

RNA-seq

Following the respective treatments, total RNA was extracted from the cells and mRNA was purified using the Dynabeads mRNA Purification Kit (Invitrogen). The purified mRNA was then fragmented and used for RNA-seq library preparation with *AccuNext* Stranded RNA-seq Library Kit for Illumina (Accurate Biology). Sequencing was conducted on an Illumina NovaSeq machine in paired-end mode with 150 bp per read (Majorbio Bio-Pharm Technology Co. Ltd., Shanghai, China).

RNA-seq data analysis

Quality control was conducted using FastQC (v0.11.9; https://www.bioinformatics.babraham.ac.uk/projects/fastqc/), and Trim Galore (v0.6.7)[69] was used for trimming low-quality bases and adapters with the parameters "–clip_R2 3 –three_prime_clip_R1 3 –clip_R1 6 –three_prime_clip_R2 6". Trimmed reads mapped to rRNAs were removed using Bowtie2 (v2.2.5).[71] The remaining reads were aligned to the human genome (hg38) using HISAT2 (v2.2.1)[72] with "–rna-strandness RF" parameters. Strand-specific reads

were separated using samtools view (v1.10)[73] with flags 99, 147, 83, and 163. Annotation files (UCSC RefSeq GRCh38) were downloaded from UCSC table browser (https://genome.ucsc.edu/). Reads on each RefSeq-annotated gene were counted using FeatureCounts (v2.0.1)[78] and normalized to transcripts per million (TPM) using R. Differentially expressed genes with adjusted *p* values of < 0.05 and fold change values of > 1.5 were identified using DESeq2 (v1.46.0).

caRNA and mRNA m^{6}A-seq

Non-ribosomal caRNAs or mRNAs were isolated from cells, and 1 μL of 1:1,000 diluted m^{6}A and non-m^{6}A spike-in from the EpiMark *N*^{6}-Methyladenosine Enrichment Kit (New England Biolabs) was added to 100 ng of purified nonribosomal caRNA or mRNA, followed by fragmentation according to previously published protocols.[9] m^{6}A-IP was performed using an EpiMark *N*^{6}-Methyladenosine Enrichment Kit. Briefly, the fragmented RNA was then incubated with Protein A/G magnetic beads (Invitrogen) conjugated to an anti-m^{6}A antibody in m^{6}A reaction buffer (150 mM NaCl, 10 mM Tris-HCl pH7.5, 0.1% NP40) with 1 U/mL RiboLock RNase inhibitor (Invitrogen) for 2 hours at 4°C with gentle rotation. Following the incubation, the bead-RNA complexes were washed stringently with low-salt reaction buffer (50 mM NaCl, 10 mM Tris-HCl pH7.5, 0.1% NP40) and high-salt reaction buffer (500 mM NaCl, 10 mM Tris-HCl pH7.5, 0.1% NP40) to remove non-specifically bound RNA. The bound m^{6}A-modified RNA was finally eluted from the beads using RLT buffer (Qiagen) and purified by RNA Clean & Concentrator-5 kit (Zymo). RNA library construction was performed using the SMARTer Stranded Total RNA-Seq Kit v2 (Takara) according to the manufacturers' respective protocols. Sequencing was conducted on an Illumina NovaSeq machine in paired-end mode with 150 bp per read (Majorbio Bio-Pharm Technology Co. Ltd., Shanghai, China).

caRNA and total mRNA m^{6}A-seq data analysis

Quality control was conducted using FastQC (v0.11.9; https://www.bioinformatics.babraham.ac.uk/projects/fastqc/), and Trim Galore (v0.6.7)[69] was used for trimming of low-quality bases and adapters with the parameters "–clip_R2 3 –three_prime_clip_R1 3 –clip_R1 6 –three_prime_clip_R2 6". rRNA-mapped reads were removed using Bowtie2 (v2.2.5).[71] The remaining reads were aligned to the human genome (hg38) along with spike-in genomes, which included two control RNAs (one with m^{6}A modifications and one without; New England Biolabs, E1610S) using HISAT2 (v2.1.1)[72] with the parameters "–rna-strandness RF". Strand-specific reads were separated using samtools view (v1.10)[73] with flags 99, 147, 83, and 163. m^{6}A peak calling was performed using macs2 (v2.2.7.1)[74] with "–keep-dup 5 -q 0.01 –nomodel" parameters. The reproducibility of m^{6}A peaks between two biological replicates was assessed using correlation plots. m^{6}A peaks identified in both two biological replicates were merged using bedtools (v.2.26.0)[75] and used in the following analysis. The m^{6}A level of each replicate was defined as the ratio of the IP sample to the input sample. Consensus motifs were analyzed using findMotifsGenome.pl in Homer (v4.11).[77]

ChIP-seq

Sonication was performed with a Qsonica Q800R3 system (Qsonica). For H3K4me3 and MYC ChIP, cells were cross-linked with 1% formaldehyde for 10 min at room temperature, and 0.125 M glycine was added to quench the reaction. The cells were then snap-frozen in liquid nitrogen and stored at −80°C. Next, 5×10^6 cells were suspended in 1 mL of ice-cold lysis buffer (50 mM HEPES, pH 7.9, 5 mM $MgCl_2$, 0.2% Triton X-100, 20% glycerol, 300 mM NaCl, and proteinase inhibitor) and incubated on ice for 10 min. The pellet was centrifuged at 500 *g* for 5 min at 4°C, suspended in 900 μL of SDS lysis buffer (50 mM HEPES, pH 7.4, 150 mM NaCl, 1 mM EDTA, 1% Triton X-100, 0.1% sodium deoxycholate, 0.1% SDS, and proteinase inhibitor), and incubated on ice for 30 min. Chromatin was sonicated at 85% amplitude with the following settings: 20 s ON and 40 s OFF for 20 min. Protein A (20 μL) and protein G (20 μL) beads were washed twice with 200 μL of SDS lysis buffer, and half of the beads were saved for preclearing. The remaining beads were resuspended in 200 μL of SDS lysis buffer, after which 5 μg of antibody and 0.5 μL of spike-in were added. The samples were then rotated at 4°C for at least 2 h. The cell lysate was centrifuged at 15,000 rpm for 10 min at 4°C and cleared using 20 μL of protein A and protein G beads for 1 h at 4°C. Five percent flow-through was saved as input, precleared lysate was mixed with antibody-coated beads, and the mixture was rotated at 4°C overnight. The next day, the flow-through was saved, and the beads were washed twice with 1 mL of SDS lysis buffer, twice with 1 mL of high-salt wash buffer (50 mM HEPES, pH 7.5, 350 mM NaCl, 1 mM EDTA, 1% Triton X-100, 0.1% sodium deoxycholate, and 0.1% SDS), twice with 1 mL of LiCl buffer (10 mM Tris-HCl, pH 8.0, 250 mM NaCl, 1 mM EDTA, 0.5% NP-40, and 0.5% sodium deoxycholate), and once with TE buffer (10 mM Tris-HCl, pH 8.0, and 1 mM EDTA) with 0.2% Triton X-100. During each wash, the sample was rotated for 5 min at 4°C. The beads were then resuspended in 240 μL of elution buffer (100 mM $NaHCO_3$ and 1% SDS) and shaken at 30°C for 1 h. The supernatant was collected, and the input was supplemented with elution buffer to a final volume of 240 μL. NaCl (5 M, 14.4 μL) was added, and the sample was shaken at 65°C for 4 h. After the addition of 4 μL of RNase A, the sample was shaken at 37°C for 15 min. Proteinase K (4 μL) was then added, and the sample was shaken at 65°C overnight. DNA was then purified by DCC with 5 × binding buffer. Purified DNA samples were prepared for sequencing using a VAHTS Universal Pro DNA Library Prep Kit for Illumina (Vayzme).

ChIP-seq data analysis

Paired-end read quality control was conducted using FastQC (v0.11.9; https://www.bioinformatics.babraham.ac.uk/projects/fastqc/), and Trim Galore (v0.6.7)[69] was used to remove low-quality bases and adapters with the parameters "–clip_R2 3 –three_prime_clip_R1 3 –clip_R1 6 –three_prime_clip_R2 6". Trimmed reads were aligned to the human (hg38) and *Drosophila melanogaster*

Please cite this article in press as: Zhang et al., FOCAS: Transcriptome-wide screening of individual m^{6}A sites functionally dissects epitranscriptomic control of gene expression in cancer, Cell (2026), https://doi.org/10.1016/j.cell.2025.11.037

(dm6) genomes using Bowtie2 (v2.2.5).[71] PCR duplicates were eliminated using MarkDuplicates from picard (v2.26.0) (http://broadinstitute.github.io/picard/). H3K4me3 peaks were identified using macs2 (v2.2.7.1),[74] and only peaks that overlapped in two biological replicates were kept for downstream analysis. Mapped reads were converted to bigwig format using Deeptools (v3.5.1)[76] bamCoverage with parameters "—binSize 5—normalizeUsing RPKM". Heatmaps and profile plots over peaks were generated using Deeptools (v3.5.1)[76] computeMatrix, plotHeatmap, and plotProfile.

RNA fragmentation followed by RIP-qPCR

Cells were collected and lysed on ice for 1 h using lysis buffer (150 mM KCl, 10 mM HEPES, pH 7.6, 2 mM EDTA, 0.5% (vol/vol) NP-40, 0.5 mM DTT, Halt protease and phosphatase inhibitors and RNase inhibitors). The lysate was then centrifuged at 13,000 rpm for 10 min at 4°C, followed by treatment with 0.1 U RNase T1 for 10 min. Protein A and protein G magnetic beads was washed twice with NT2 buffer (200 mM NaCl, 50 mM HEPES, pH 7.6, 2 mM EDTA, 0.05% (vol/vol) NP-40, 0.5 mM DTT, and Halt protease and phosphatase inhibitors, and RNase inhibitors) to be prepared and resuspended in 200 μL of NT2 buffer. Half of the beads were used for IP by adding the appropriate antibody and rotating at 4°C for at least 2 h. The other half was used for preclearing by adding to the cell lysate, and the mixture was incubated by rotation at 4°C for 30 min. The supernatant was transferred to a new tube after magnetically separating the beads. The antibody beads were washed three times with NT2 buffer and added to the cleaned cell lysate. The mixture was rotated overnight at 4°C, the supernatant was resuspended in 1 mL of TRIzol reagent (Invitrogen), and the RNA was extracted. Notably, all consumables and buffer used were guaranteed to be RNA enzyme free and were supplemented with RNA enzyme inhibitors. All primers used for RIP-qPCR assays are listed in Table S1, and relative expression was calculated using the $\Delta\Delta C_t$ method.

RNA transcription rate assay

Nascent RNA was isolated according to a previously published procedure.[80] Briefly, 5×10^5 cells were collected and labeled with 100 μM 5-ethynyl uridine (EU) for 1 h to mark newly synthesized RNA, followed by biotinylation using click chemistry following the recommended procedure. Biotinylated RNA samples were recovered through ethanol precipitation, and nascent transcripts were isolated using streptavidin beads. Beads were resuspended using 0.5 mg of proteinase K (Invitrogen) and 25 μL of 2 × proteinase K buffer (100 mM Tris-HCl, 150 mM NaCl, 12.5 mM EDTA, and 2% (wt/vol) SDS) and incubated at 55°C for 30 min. The flowthrough was saved, and beads were resuspended in 50 μL of RNase-free water, followed by incubation at 70°C for 30 min. The flowthrough was saved and purified together with the flowthrough from the previous step using an RNA Clean & Concentrator-5 kit (Zymo). RT-qPCR was then performed on a LightCycler 480 II system (Roche) using Taq Pro Universal SYBR qPCR Master Mix (Vazyme).

RNA lifetime measurement by qPCR

dPspCas13b-*wt*FTO cells of four cancer cell lines were seeded in a 12-well plate, and after 24 h, actinomycin D was added at a concentration of 2 μg/mL at 8, 4, and 0 h before trypsinization and collection. For transcripts with shorter RNA half-lives, actinomycin D was added at 2 μg/mL at 4, 2, and 0 h. Total RNA was isolated using RNA isolator total RNA extraction reagent (Vayzme). Before determining RNA quantities by RT-qPCR, 1 μL of 1:100 diluted m^{6}A and non-m^{6}A spike-in from the EpiMark *N*^{6}-Methyladenosine Enrichment Kit (New England Biolabs) was added.

Colony formation assay

In each well of a six-well culture plate, 1,500 cells were seeded, with three replicates per group. After incubation for 7 to 14 days, the culture medium was aspirated, and the cells were rinsed twice with 1 × PBS. Subsequently, cells were fixed with 4% paraformaldehyde for 20 min, stained with 0.1% crystal violet (in 25% methanol) for 20 min, washed with water, and air dried. Colonies were manually counted.

Wound healing assay

For the scratch wound assay, 3×10^5 SMMC-7721 cells per well (three replicates per group) were seeded into a six-well plate and incubated until confluent. The cell monolayer was then scratched using a pipette tip and washed with serum-free medium to remove detached cells. Images of the scratched area were captured at 0, 6, and/or 12 h after wounding (Zesis, AXIO). Percent wound closure was calculated as migration area (%) = $(A_0 - A_n)/A_0 \times 100$, where A_0 represents the initial wound area, and A_n represents the remaining wound area at the designated time point.

Transwell assay

In the transwell assay, 1×10^4 SMMC-7721 cells per well (three replicates per group) were suspended in low-serum (5% FBS) medium and seeded into the top chamber of 24-well transwell plates (Corning, Corning, NY, USA) with 8-μm pore filters. The bottom chamber was then filled with complete medium (containing 10% FBS). After 24 h, cells attached to the upper surface of the filter

membranes were removed, and migrated cells on the lower surface were stained with 0.5% crystal violet for several minutes. Migration levels were observed under an optical microscope (Leica DMI6000B, Germany).

Definition and quantification of carRNAs

We identified chromatin-associated regulatory RNAs (carRNAs), including repeats RNAs (reRNAs), enhancer RNAs (eRNAs), and promoter-associated RNAs (paRNAs), based on previous work.[9] Annotation of reRNAs for hg38 was obtained from the UCSC Table Browser (https://genome.ucsc.edu/cgi-bin/hgTables). Acetylation of histone H3 at lysine 27 (H3K27ac) peaks were called using H3K27ac ChIP-seq in SMMC-7721 cells (GEO: GSE119086), HepG2 cells (GEO: GSE29611), HCT116 cells (GEO: GSE96299), and HeLa cells (GEO: GSE96299) by macs2 (v2.2.7.1)[74] with "—keep-dup 5 -q 0.01" parameters. Read counts were quantified using FeatureCounts (v2.0.1),[78] and TPM normalization was performed based on sequencing depth. Only carRNAs with a minimum of 10 reads in both input samples were retained for subsequent analysis. m^{6}A levels of those carRNAs were normalized with library depth and calculated as $\log_2$ (IP/input).

sgRNA type definition

sgRNAs within m^{6}A peaks identified by caRNAs m^{6}A-seq were annotated using the carRNAs (eRNAs, paRNAs, and reRNAs) bed files separately and the "bedtools intersect -s" command. sgRNAs that were annotated to multiple types of carRNAs were prioritized based on the following order: paRNA > reRNA > eRNA. For the remaining sgRNAs not classified as carRNAs and those located solely within m^{6}A peaks detected by total RNA m^{6}A-seq, annotation was performed based on the protein coding gene that they were associated with.

Quantification of m^{6}A-mediated regulatory strength and concordance between cell lines

To assess the cross-lineage regulatory relevance of m^{6}A-modified sites, we quantified the regulatory intensity and inter-lineage concordance of m^{6}A-associated motifs shared between SMMC-7721 and HepG2 cell lines. We first identified shared RRACH motifs (putative m^{6}A consensus sites) present in both cell lines. Among these, we defined a motif as effective if it was targeted by at least one significantly enrich or dropout sgRNA in either cell line, based on FOCAS.

For each effective motif, we collected all significant sgRNAs (adjusted $p < 0.05$) that target the motif in a given cell line and computed the arithmetic mean of their RRA scores. This value reflects the regulatory potential of m^{6}A modification at that motif within the context of CRISPR perturbation. Next, all effective motifs were grouped by their associated target gene, and the following gene-level features were computed:

(1) **m^{6}A intensity**, defined as the root-mean-square (RMS) of mean RRA scores of all motifs linked to the gene ***g*** in cell line ***c***. For each gene ***g***, let there be ***N*** motifs targeted by significant sgRNAs. Each motif ***j*** is targeted by n_j significant sgRNAs in cell line ***c***, with RRA scores denoted as $RRA_{i,j,c}$, where i=1, …, n_j. The **m^{6}A intensity** of gene ***g*** in cell line ***c*** is calculated as follows:

$$Intensity(g,c) = \sqrt{\frac{1}{N}\sum_{j=1}^{N}\left(\frac{1}{n_j}\sum_{i=1}^{n_j} RRA_{i,j,c}\right)}$$

(2) **Inter-lineage regulatory concordance**. To allow for meaningful cross-gene comparison, intensity values were min-max normalized within each cell line:

$$Intensity_{norm}(g,c) = \frac{Intensity(g,c) - \min\left(Intensity(c)\right)}{max(Intensity(c)) - \min\left(Intensity(c)\right)}$$

Assume that for a gene ***g***, there are ***n*** common motifs in cell line A (e.g., SMMC-7721) and cell line B (e.g., HepG2), and their corresponding mean RRA values are two vectors:

$$RRA_A = \left[r_{A,1}, r_{A,2}, \ldots r_{A,n}\right], RRA_B = \left[r_{B,1}, r_{B,2}, \ldots r_{B,n}\right]$$

where $\mathbf{r_{A,i}}$ is the mean RRA of a motif ***i*** in cell line A and $\mathbf{r_{B,i}}$ is the mean RRA of the same motif in cell line B. Then the RRA correlation of this gene ***g*** between the two cell lines A and B is:

$$Correlation_{A,B}(g) = \frac{\sum_{i=1}^{n}\left(r_{A,i} - \bar{r}_A\right)\left(r_{B,i} - \bar{r}_B\right)}{\sqrt{\sum_{i=1}^{n}\left(r_{A,i} - \bar{r}_A\right)^2 \sum_{i=1}^{n}\left(r_{B,i} - \bar{r}_B\right)^2}}$$

Please cite this article in press as: Zhang et al., FOCAS: Transcriptome-wide screening of individual m^{6}A sites functionally dissects epitranscriptomic control of gene expression in cancer, Cell (2026), https://doi.org/10.1016/j.cell.2025.11.037

where $\bar{\mathbf{r}}_{\boldsymbol{A}}$ and $\bar{\mathbf{r}}_{\boldsymbol{B}}$ are the means of the vectors $\mathbf{RRA}_A$ and $\mathbf{RRA}_B$. Genes with fewer than two shared motifs or with no variance in motif scores were excluded from this calculation. Finally, the **inter-lineage regulatory concordance** score for each gene ***g*** was computed as the product of the normalized regulatory intensities in both cell lines and their inter-lineage RRA correlation coefficient:

$$Regulatory\ Concordance(g) = Intensity_{norm}(g, SMMC7721) \times Intensity_{norm}(g, HepG2) \times Correlation_{SMMC7721,HepG2}(g)$$

This composite metric integrates the strength and consistency of regulatory signals across two lineages. Genes with high concordance scores are likely to contain m^{6}A modifications with robust and conserved regulatory effects.

Identification of common differential PanPeaks and integrated zLFC quantification

We systematically identified PanPeaks with unanimous directional changes across a set of cell lines

$$C = \{cell_1, \ldots, cell_n\}$$

A PanPeak ***p*** was classified as consensus directional (either "dropout" or "enrich") if it satisfied:

$$\forall i \in C, direction_i(p) = d, where\ d \in \{dropout, enrich\}$$

For each consensus PanPeak ***p***, we quantified its regulatory impact through the following steps:

(1) Cell line-specific zLFC aggregation: For each cell line $\boldsymbol{i} \in C$, we summed the *z*-score of $\log_2$FoldChange (zLFC) values of effective sgRNAs associated with PanPeak ***p*** and direction ***d***

$$zLFC_i(p, d) = \sum_{g \in G(p,d,i)} zLFC_g, \forall i \in C$$

where $G(p, d, i)$ denotes the set of sgRNAs targeting PanPeak ***p*** with direction ***d*** in cell line ***i***.

(2) Integrated regulatory score: The multi-cell zLFC score was calculated as the mean across all cell lines

$$zLFC_{intergrated}(p) = \left| \frac{1}{|C|} \sum_{i \in C} zLFC_i(p, d) \right|$$

where $|C| = n$ represents the total number of cell lines.

Enrichment analysis

GO enrichment analysis was performed with Metascape[81] and David[82,83] with default parameters.

QUANTIFICATION AND STATISTICAL ANALYSIS

Plots were generated using GraphPad Prism software v9.0, unless otherwise stated. R packages used in all analyses are indicated in their respective STAR Methods sections, along with the statistical tests used. Unless otherwise specified, all statistical tests were performed using GraphPad Prism software. The paired *t*-test was used for comparing two groups.

n indicates the number of biological replicates. Error bars indicate mean ± S.D. *P* values less than 0.05 were considered significant for all statistical analyses. For comparisons between two groups, paired data were analyzed using two-tailed paired Student's *t*-tests, while unpaired data were analyzed using Wilcoxon rank-sum tests.

The open-source ImageJ software was used to quantitate the immunoblotting. The normalized intensities, represented as bar graphs, were calculated by comparing the intensity of the proteins of interest to that of H3.

CellPress

Supplemental figures

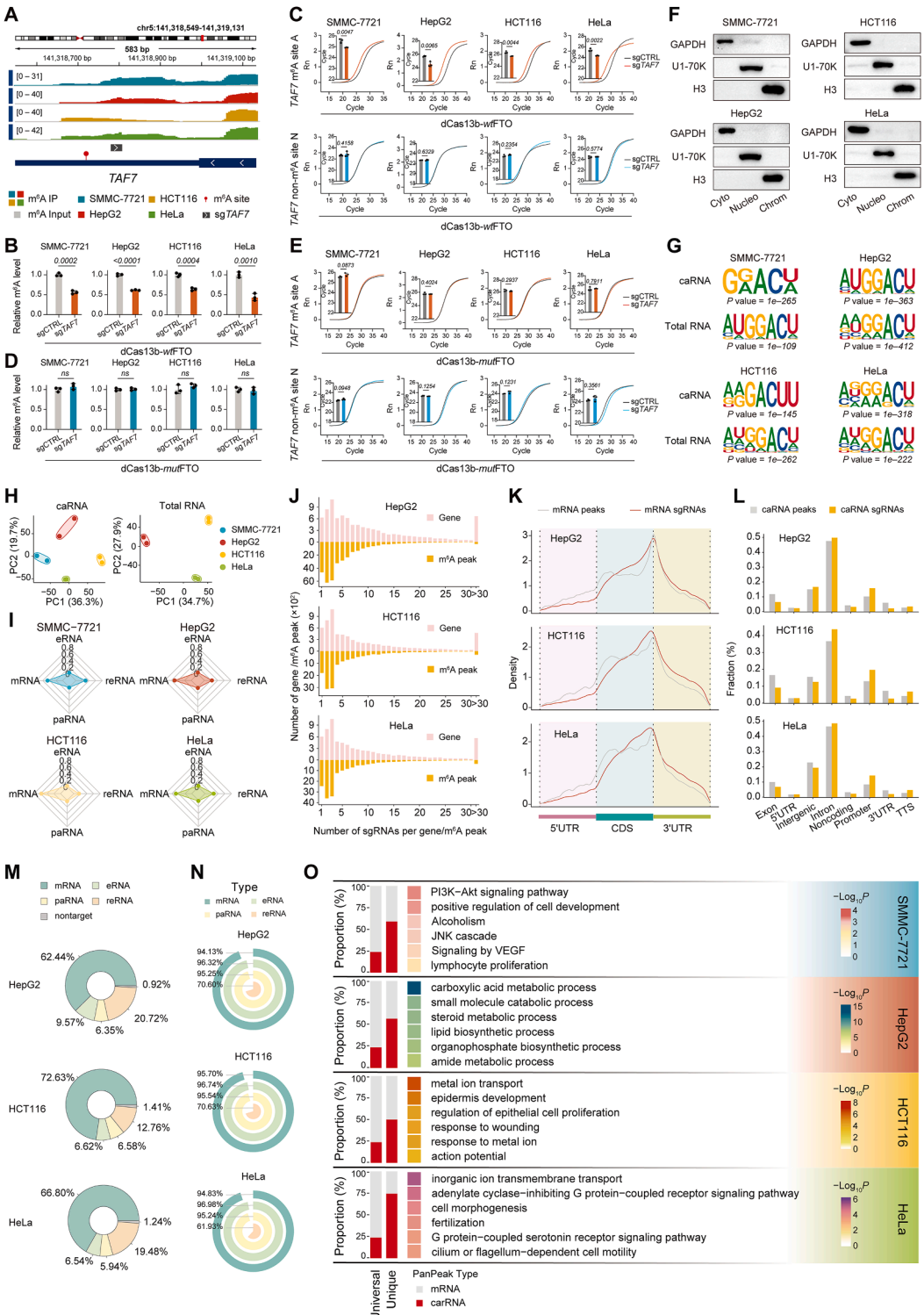

(legend on next page)

Figure S1. System validation, m^{6}A-seq quality control, and characterization of sgRNA libraries, related to Figure 1

(A) m^{6}A peaks at targeted m^{6}A sites on *TAF7* mRNA.

(B–E) *TAF7* methylation levels assessed by MeRIP-qPCR (B and D) and SELECT-qPCR (C and E) in four cell lines expressing dCas13b-*wt*FTO (B and C) and dCas13b-*mut*FTO (D and E) with sg*TAF7* versus nontarget sgRNA (n = 3).

(F) Immunoblot showing cytoplasmic, nuclear, and chromatin fractionation in four cell lines.

(G) Enriched consensus motif from m^{6}A peaks across four cell lines.

(H) Principal-component analysis (PCA) of global m^{6}A levels in four cell lines.

(I) Distribution of m^{6}A peak-associated RNA types across four cell lines.

(J) Distribution of sgRNAs targeting each gene (top) and each m^{6}A peak (bottom) in HepG2, HCT116, and HeLa cells.

(K) mRNA m^{6}A peaks and sgRNA library distribution along transcripts in HepG2, HCT116, and HeLa cells.

(L) Proportion of caRNA m^{6}A peaks and the sgRNA library across genomic regions in HepG2, HCT116, and HeLa cells.

(M) Proportion of sgRNAs targeting different RNA types and nontarget sgRNAs in HepG2, HCT116, and HeLa cells.

(N) Coverage of m^{6}A peaks by the sgRNA libraries across different RNA types in HepG2, HCT116, and HeLa cells.

(O) Proportion of RNA types in universal and unique PanPeaks (left), and GO analysis for genes with unique PanPeaks (right).

Error bars indicate mean ± SD (B–E). ns, not significant (D).

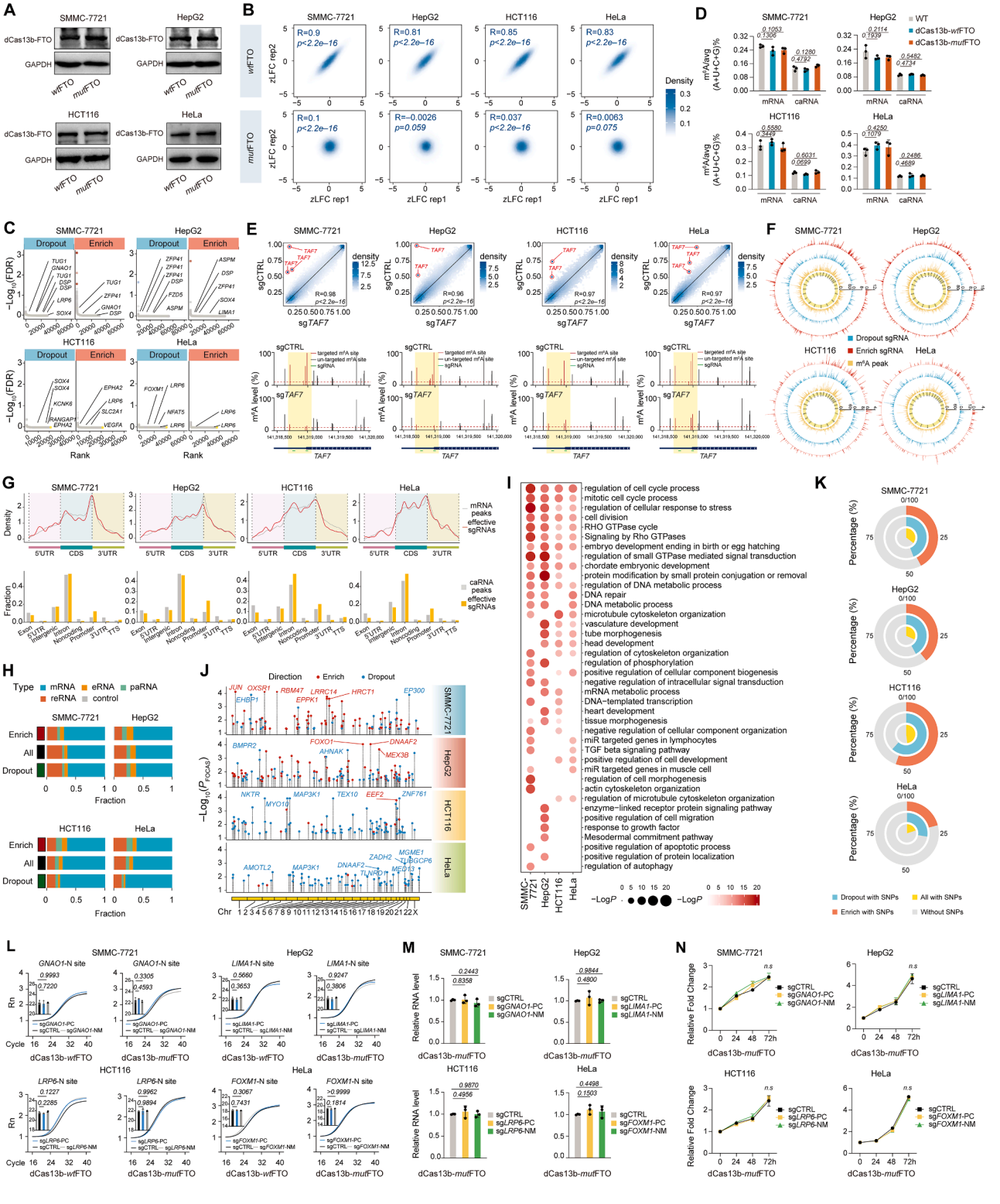

Figure S2. dCas13b-*mut*FTO control, off-target analysis, and effective sgRNA feature profiling across four cell lines, related to Figure 2

(A) dCas13b-FTO expression levels in four cell lines expressing dCas13b-*wt*FTO and dCas13b-*mut*FTO.

(B) *z*LFC of sgRNAs in two independent biological replicates across four cell lines expressing dCas13b-*wt*FTO (top) or dCas13b-*mut*FTO (bottom) at 14 D_t after sgRNA transduction.

(C) sgRNA ranking by RRA across four cell lines expressing dCas13b-*mut*FTO. Known cancer-associated m^6A genes are labeled.

(legend continued on next page)

(D) LC-MS/MS quantification of the m^6A ratios in mRNAs and non-ribosomal caRNAs from cells transfected with dCas13b-FTO (wild type or mutant, $n = 3$).
(E) m^6A ratios of all m^6A sites in dCas13b-*wt*FTO cells treated with sg*TAF7* (green lines) versus nontarget sgRNA (top) detected using glyoxal and nitrite-mediated deamination of unmethylated adenosines sequencing (GLORI-seq). m^6A ratio of m^6A sites within (yellow-highlighted) and beyond the sgRNA targeting region of *TAF7* mRNA (bottom).
(F) Read density of m^6A peaks and effective sgRNAs across the genome in four cell lines.
(G) mRNA m^6A peaks and effective sgRNA distribution along transcripts in four cell lines (top). Proportion of caRNA m^6A peaks and effective sgRNAs across genomic regions in four cell lines (bottom).
(H) Fraction of sgRNAs targeting different RNA species or nontarget controls (<2%) across four cell lines.
(I) GO analysis of FiGenes in each cell line.
(J) Distribution of mDM sites covered by effective sgRNAs located ±200 bp from the site in each cell line.
(K) Proportion of genes with or without SNPs targeted by dropout and enrich candidates across cell lines.
(L) SELECT-qPCR validating m^6A reduction at adjacent N sites in dCas13b-*wt*FTO or dCas13b-*mut*FTO cells with effective sgRNAs versus controls.
(M–N) RT-qPCR (M) and CCK-8 assay (N) measuring transcript-level changes and cell proliferation in dCas13b-*mut*FTO cells with effective sgRNAs versus controls ($n = 3$).
Pearson correlation coefficient (R) and *p* value are shown in (B) and (E). Error bars indicate mean ± SD (D and L–N). ns, not significant (N).

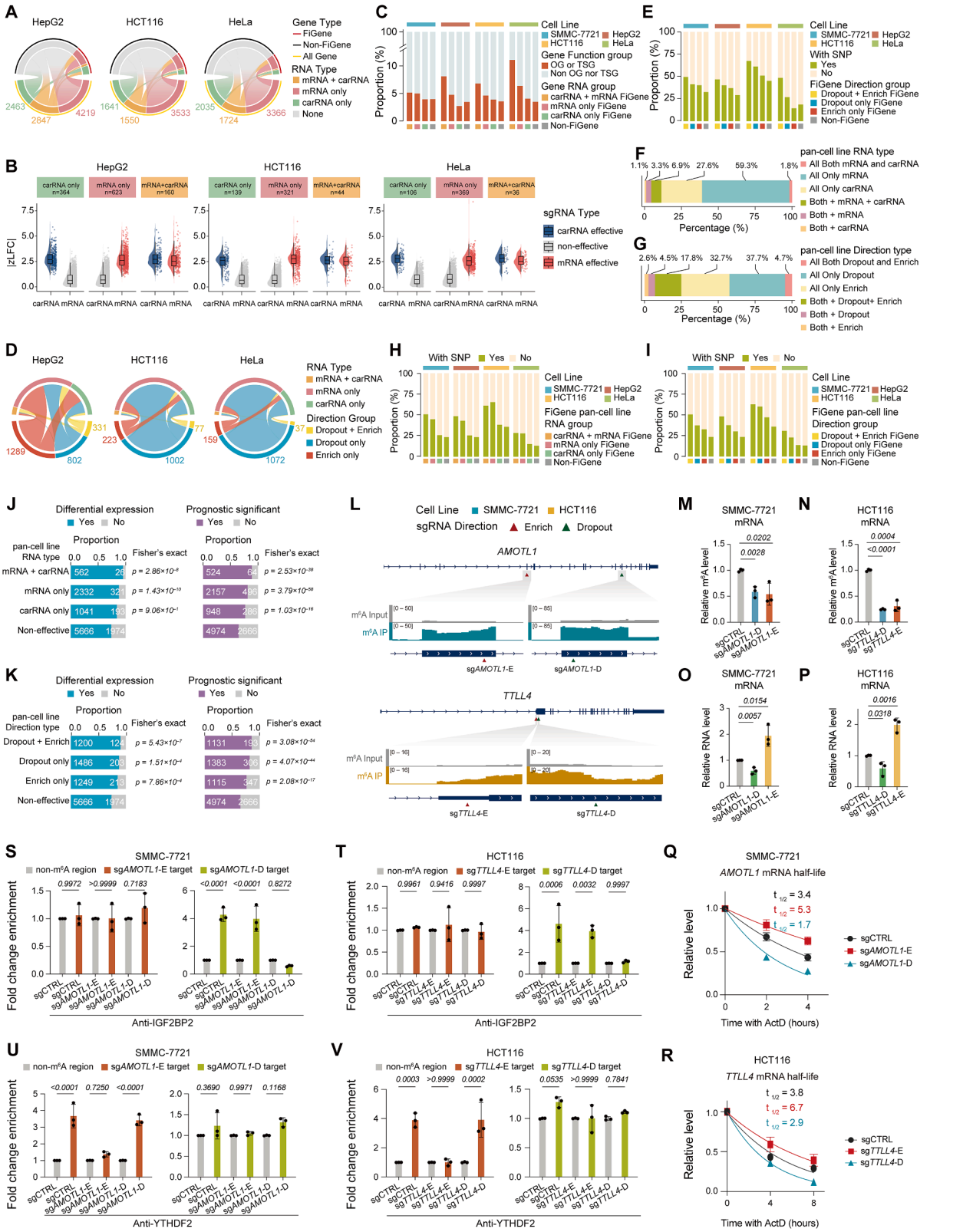

(legend on next page)

Figure S3. Analysis and validation of FiGenes regulated by multiple RNA types and in opposite directions, related to Figure 3

(A) Distribution of RNA types targeted by multiple sgRNAs within the same gene across FiGenes and non-FiGenes in HepG2, HCT116, and HeLa cells.

(B) zLFC for sgRNAs targeting carRNA or mRNA within FiGenes in HepG2, HCT116, and HeLa cells. FiGenes are grouped by effective sgRNA RNA type.

(C) Proportion of OGs or TSGs, as defined by the COSMIC CGC, among FiGenes grouped by effective sgRNA RNA types across four cell lines.

(D) Distribution of sgRNA RNA types and direction types for FiGenes in HepG2, HCT116, and HeLa cells.

(E) Proportion of FiGenes with cancer-related SNPs grouped by effective sgRNA direction types across four cell lines.

(F and G) Proportion of FiGenes categorized by RNA types (F) or direction types (G) of effective sgRNAs on a pan-cell line level.

(H and I) Proportion of FiGenes with cancer-related SNPs grouped by effective sgRNA RNA types (H) or direction types (I) at the pan-cell line level across four cell lines.

(J and K) Proportion of FiGenes with altered expression in tumors versus normal tissues (J) and associated with survival outcomes (K) from the OncoDB website (left) and the Human Protein Atlas website (right), grouped by sgRNA RNA types (J) or direction types (K). Statistical significance was determined by Fisher's exact test.

(L) m^6A peaks on *AMOTL1* (SMMC-7721) and *TTLL4* (HCT116), with effective sgRNAs (enrich: sg-*AMOTL1*-E/sg*TTLL4*-E, red; dropout: sg-*AMOTL1*-D/sg*TTLL4*-D, green).

(M–P) Methylation levels (M and N) and transcript levels (O and P) of *AMOTL1* (M and O) and *TTLL4* (N and P) were assessed using MeRIP-qPCR and RT-qPCR in dCas13b-*wt*FTO cells with corresponding sgRNAs versus nontarget sgRNA ($n = 3$).

(Q and R) mRNA half-life of *AMOTL1* (Q) and *TTLL4* (R) was assessed by RT-qPCR after actinomycin D treatment in SMMC-7721- and HCT116-dCas13b-*wt*FTO cells with sgRNAs targeting *AMOTL1* (Q) or *TTLL4* (R) versus nontarget sgRNA ($n = 3$).

(S–V) The binding of IGF2BP2 (S and T) and YTHDF2 (U and V) to specific *AMOTL1* (S and U) or *TTLL4* (T and V) regions was assessed by fragmented RIP-qPCR in SMMC-7721- or HCT116- dCas13b-*wt*FTO cells with sgRNAs targeting *AMOTL1* or *TTLL4* versus nontarget sgRNA, comparing the enrichment at the targeted m^6A regions versus non-methylated regions ($n = 3$).

Error bars indicate mean ± SD (M–V).

(legend on next page)

Figure S4. Cross-cell line analysis of PanPeaks and characterization of FiGenes and FiPeaks, related to Figure 4

(A) Absolute zLFC values of FiPeaks across four cell lines. Statistical significance was assessed by Wilcoxon rank-sum test.

(B) Proportion of OGs or TSGs, as defined by CGC, among FiGenes across four cell lines.

(C) Proportion of FiGenes harboring cancer-related SNPs across four cell lines.

(D and E) Proportion of FiGenes associated with significantly altered expression in tumors versus normal tissues from the OncoDB (D) or associated with distinct patient survival outcomes from the Human Protein Atlas (E). Statistical significance was determined by Fisher's exact test.

(F and G) Distribution of FiGenes based on pan-cell line RNA types (F) or sgRNA direction types (G).

(H) Heatmaps of PanPeak features grouped by the overlap between FOCAS screening efficacy and peak presence across cell lines. Each group shows the following features for each PanPeak (from top to bottom): FOCAS screening result, m^6A modification levels, and RNA expression levels.

(I and J) Violin plot and boxplot showing m^6A levels (I) and RNA expression levels (J) of unique FiPeaks from universal PanPeaks across four cell lines. Statistical significance was assessed by Wilcoxon rank-sum test.

(K) Dot plot showing m^6A peak occurrence rates within PanPeaks regions, grouped by FiPeak types across various organs.

(L) Mean expression levels of FiGenes across different developmental time points in each tissue, early embryos, and human embryonic stem cells (hESCs).

(M) Jaccard index quantifying FiGenes overlap between cell line pairs.

(N) FiGenes with shared FiPeaks in liver cancer cell lines and the screening outcomes of their FiPeaks in HCT116 and HeLa cells.

(O) m^6A intensity of FiGenes in SMMC-7721 (red) and HepG2 (blue) cells, along with inter-lineage regulatory concordance (green) between the two cell lines. Genes with known relevance in liver cancer, based on differential expression in tumors versus normal tissue, reported roles, or association with patient survival, are labeled.

(P) Kaplan-Meier disease-free survival for LIHC patients stratified by *ANKRD18A*, *JPT2*, and *CDK14* expression (Benjamini-Hochberg-adjusted log-rank test). Sample sizes (high-low expression): *ANKRD18A*, n = 260–287; *JPT2*, n = 91–90; *CDK14*, n = 345–345.

(Q–S) RNA levels and m^6A profiles within the liver-cancer unique PanPeaks: PanPeak-coding-13061 associated with *ANKRD18A* mRNA (Q), PanPeak-coding-4726 associated with *JPT2* mRNA (R), and PanPeak-ca-12172 associated with L1HS reRNA in the intron of *CDK14* (S) across four cell lines.

(T–V) MeRIP-qPCR (T), CCK-8 (U), and colony formation (V) assays measuring m^6A levels and cell proliferation in dCas13b-*wt*FTO cells transfected with sg*ANKRD18A*, sg*JPT2*, or sg*CDK14* versus nontarget sgRNA across four cell lines (n = 3, $^*p < 0.05$, $^{**}p < 0.01$, $^{****}p < 0.0001$, error bars indicate mean ± SD; ns, not significant).

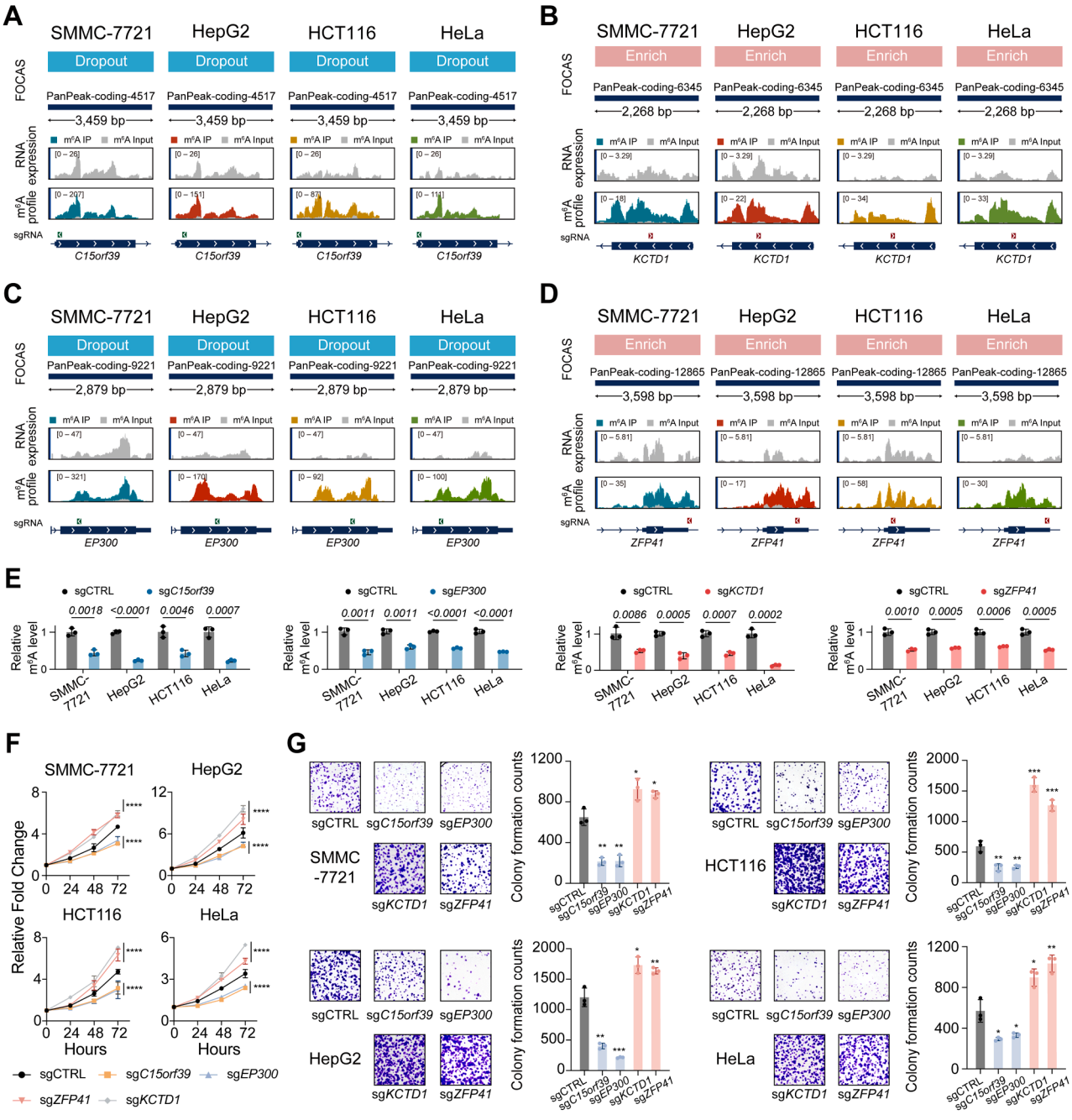

Figure S5. Analysis and validation of liver-cancer unique and universal FiGenes, related to Figure 5

(A–D) RNA levels and m^{6}A profiles within the universal FiPeaks: PanPeak-coding-4517 associated with *C15orf39* mRNA (A), PanPeak-coding-6345 associated with *KCTD1* mRNA (B), PanPeak-coding-9221 associated with *EP300* mRNA (C), and PanPeak-coding-12865 associated with *ZFP41* mRNA (D) across four cell lines.

(E–G) MeRIP-qPCR (E), CCK-8 (F), and colony formation (G) assays measuring m^{6}A levels and cell proliferation in cells transfected with sg*C15orf39*, sg*KCTD1*, sg*EP300*, or sg*ZFP41* versus nontarget sgRNA across four cell lines ($n = 3$, *$p < 0.05$, **$p < 0.01$, ***$p < 0.001$, ****$p < 0.0001$, error bars indicate mean ± SD).

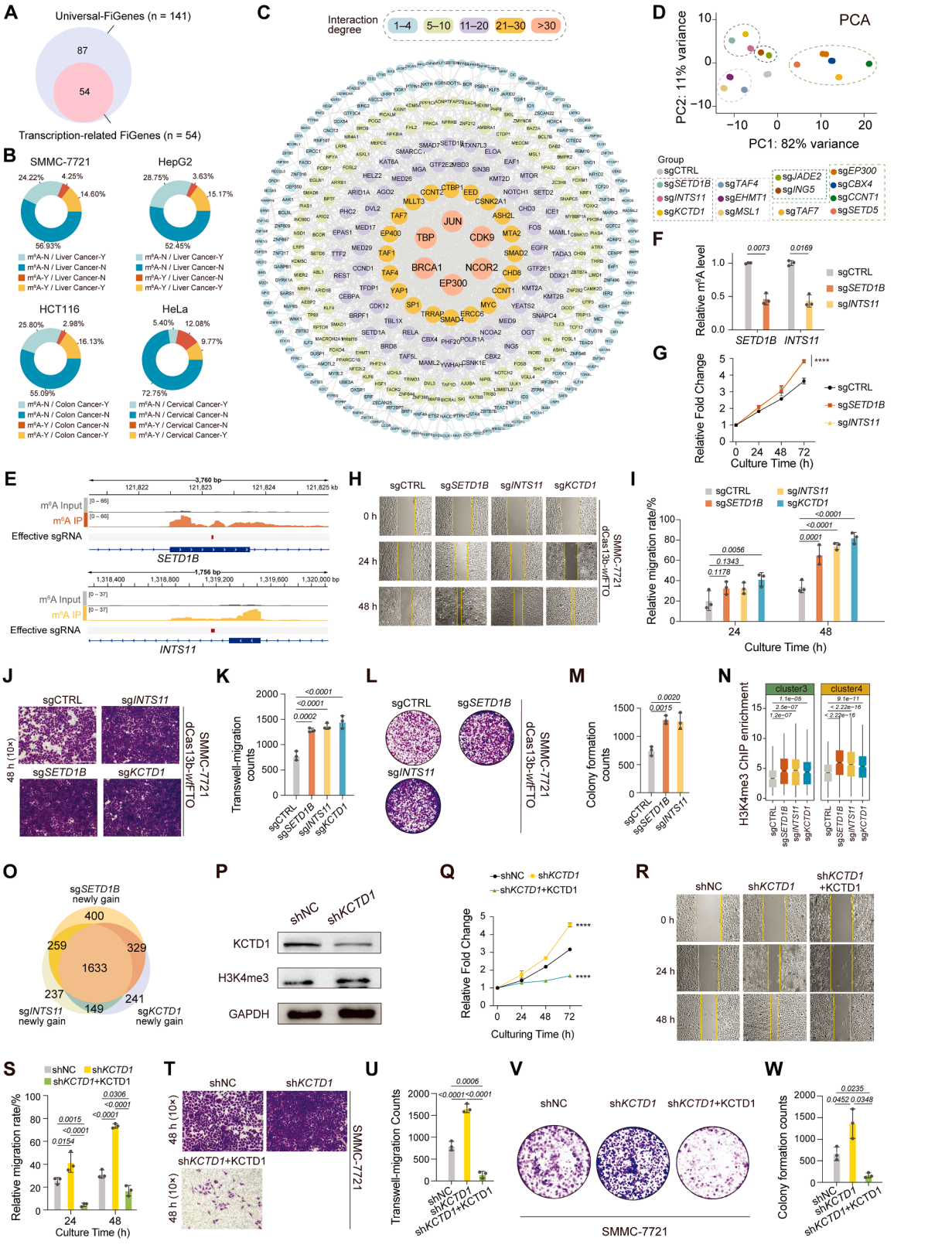

(legend on next page)

Figure S6. Analysis of transcription-related FiGenes and functional investigation of E1 module FiGenes in SMMC-7721 cells, related to Figure 6

(A) Proportion of transcription-related FiGenes among universal FiGenes.

(B) Proportion of transcription-related FiGenes that are or are not associated with m^6A modification (m^6A-Y: previously reported to be regulated by m^6A; m^6A-N: no published studies reported m^6A-dependent regulation of the gene) and the corresponding cancer type (Cancer-Y: reported to play a functional role in the corresponding cancer; Cancer-N: not previously linked to the cancer) in each of the four cell lines.

(C) STRING-derived PPI network of transcription-related common FiGenes. Node size reflects interaction degree, and colors denote clusters.

(D) PCA of gene expression in SMMC-7721-dCas13b-*wt*FTO cells with sgRNAs targeting selected transcription-related FiGenes versus nontarget sgRNA.

(E) m^6A peaks on *SETD1B* and *INTS11* in SMMC-7721 cells with the corresponding effective sgRNAs.

(F) MeRIP-qPCR measuring *SETD1B* and *INTS11* methylation in dCas13b-*wt*FTO cells with sg*SETD1B* or sg*INTS11* versus nontarget sgRNA ($n = 3$).

(G–M) CCK-8 assay (G), wound healing (H and I), transwell (J and K), and colony formation (L and M) assays showing proliferation, migration, and clonogenicity of SMMC-7721-dCas13b-*wt*FTO cells with sg*SETD1B* or sg*INTS11* versus nontarget sgRNA ($n = 3$, $^{****}p < 0.0001$).

(N) H3K4me3 enrichment (±1 kb TSSs) in cluster 3 and cluster 4 genes of SMMC-7721 cells with E1 module sgRNAs versus nontarget sgRNA. Statistical significance was assessed by Wilcoxon rank-sum test.

(O) Overlap among genes that newly gained H3K4me3 peaks after E1 module sgRNA treatment versus nontarget sgRNA.

(P) Protein levels of H3K4me3 and KCTD1 in SMMC-7721 cells transfected with control short hairpin RNA (shRNA) (shNC) or shRNA targeting *KCTD1* (sh*KCTD1*).

(Q–W) CCK-8 (Q), wound healing (R–S), transwell (T–U), and colony formation (V–W) assays showing effects of sh*KCTD1* or sh*KCTD1*+*KCTD1* rescue on proliferation, migration, and clonogenicity in SMMC-7721 cells ($n = 3$, $^{****}p < 0.0001$).

Error bars indicate mean ± SD (E, F, I, J, M, Q, S, U, and W). Scale bar: 200 μm in (H), (J), (R), and (T).